OPEN ACCESS Freely available online

PLoS one

Visualization of Painful Experiences Believed to Trigger the Activation of Affective and Emotional Brain Regions in Subjects with Low Back Pain

Kazuhiro Shimo[1], Takefumi Ueno[2], Jarred Younger[3], Makoto Nishihara[1], Shinsuke Inoue[1], Tatsunori Ikemoto[4], Shinichirou Taniguchi[5], Takahiro Ushida[1,5]*

1 Multidisciplinary Pain Center, Aichi Medical University, Aichi, Japan, **2** Department of Neuropsychiatry, Kyushu University, Fukuoka, Japan, **3** Department of Anesthesia, School of Medicine, Stanford University, Stanford, California, United States of America, **4** NPO Pain Medicine Research Information Center, Kochi, Japan, **5** Department of Orthopaedic Surgery, Kochi Medical School, Kochi, Japan

Abstract

In the management of clinical low back pain (LBP), actual damage to lower back areas such as muscles, intervertebral discs etc. are normally targeted for therapy. However, LBP may involve not only sensory pain, but also underlying affective pain which may also play an important role overall in painful events. Therefore we hypothesized that visualization of a painful event may trigger painful memories, thus provoking the affective dimension of pain. The present study investigated neural correlates of affect processing in subjects with LBP (n = 11) and subjects without LBP (n = 11) through the use of virtual LBP stimuli. Whole brain functional magnetic resonance imaging (MRI) was performed for all subjects while they were shown a picture of a man carrying luggage in a half-crouching position. All subjects with LBP reported experiencing discomfort and 7 LBP subjects reported experiencing pain. In contrast to subjects without LBP, subjects with LBP displayed activation of the cortical area related to pain and emotions: the insula, supplementary motor area, premotor area, thalamus, pulvinar, posterior cingulate cortex, hippocampus, fusiform, gyrus, and cerebellum. These results suggest that the virtual LBP stimuli caused memory retrieval of unpleasant experiences and therefore may be associated with prolonged chronic LBP conditions.

Citation: Shimo K, Ueno T, Younger J, Nishihara M, Inoue S, et al. (2011) Visualization of Painful Experiences Believed to Trigger the Activation of Affective and Emotional Brain Regions in Subjects with Low Back Pain. PLoS ONE 6(11): e26681. doi:10.1371/journal.pone.0026681

Editor: Kazutaka Ikeda, Tokyo Metropolitan Institute of Medical Science, Japan

Received July 1, 2011; **Accepted** October 2, 2011; **Published** November 2, 2011

Funding: This work was supported by a Grant-in-Aid for Scientific Research from the Ministry of Health, Labour, and Welfare. The funders had no role in study design, data collection and analysis, decision to publish, or preparation of the manuscript.

Competing Interests: The authors have declared that no competing interests exist.

* E-mail: ushidat-koc@umin.ac.jp

Introduction

Psychological factors are known to affect the subjective experience of pain. Pain catastrophizing is one such maladaptive response to pain that is characterized by heightened pain intensity [1], increased disability [2]and difficulty disengaging from pain [3]. Recently, functional neuroimaging techniques have been developed that allow the neural correlates of psychological states to be explored. The blood oxygenation level-dependent contrast (BOLD-fMRI) is currently the most popular tool for mapping human brain activity [4]. Pain-related brain activations which could be considered as psychological factors have been reported in various studies. In healthy volunteers, several brain regions, including the primary and secondary somatosensory cortices, insula, anterior cingulate cortex (ACC), thalamus, and motor cortex, respond to real noxious stimuli and are regarded as part of the "pain matrix" [5,6]. However, it is also known that the expectation of pain can evoke brain activation patterns resembling that of a real pain experience [7].

In a previous study [8,9], Ogino reported that the imagination of pain even without physical injury engages the cortical representations of the pain-related neural network. Also, we reported that prior pain experiences can strongly affect pain anticipation and associated brain activations. We have also found that the anticipation of painful stimuli can cause the activation of cortical areas underlying pain-related affect in chronic neuropathic pain patients [10]. Activation in the brain during the visualization of a painful experience was found in the ACC and the medial prefrontalcortex (MPFC), which are regions known to be areas associated with pain and affect processing. Similar activations were found to be correlated with pain catastrophizing in individuals with fibromyalgia [11]. In that study, pain catastrophizing was associated with greater activity in the dorsolateral prefrontal cortex, rostral ACC, and MPFC, regions implicated in pain vigilance, attention and awareness [12,13,14,15]. These results suggest that pain-related neuronal activities might reflect the development and maintenance of chronic pain syndromes.

Low back pain (LBP) is one of the most common chronic pain syndromes. A recent fMRI study in humans reported actual LBP-related cerebral substrates [16]. Abnormal activations were identified in the prefrontal cortex, insula, thalamus, posterior cingulate cortex (PCC), supplementary motor area (SMA), and premotor areas (PMA) – predominantly in the right hemisphere.

Table 1. Evaluations of task-related discomfort and pain.

	LBP group (n=11)	non-LBP group(n=11)
Experiences evoked by tasks		
Discomfort (range)	3.5 (1–6)	0
Pain (range)	2.1 (0–6)	0
RDQ (mean ± SD)	3.1±3.1	0
ODI (mean ± SD)	19.8±7.8%	0

RDQ, Roland-Morris Disability Questionnaire; ODI, Oswestry Disability Index 2.0.
doi:10.1371/journal.pone.0026681.t001

We hypothesized that visualization of a painful experience would provoke unpleasant emotions, and these emotions might have a role in the maintenance of chronic pain syndromes. The present study investigated neural correlates of affect processing in subjects with nonspecific LBP and subjects without LBP by using virtual visual stimuli.

Results

Self-reported discomfort and pain (Table 1)

All subjects in the LBP group reported discomfort associated with viewing the simulated back pain (mean NRS score, 3.5; range, 1–6). 7 of the 11 subjects in the LBP group described pain associated with the task. However, no subjects in the non-LBP group reported any discomfort or pain resulting from viewing the picture of back pain.

fMRI results

Compared with the non-LBP group, the LBP group demonstrated significantly more activation in the left fusiform, as well as left inferior temporal gyrus, bilateral precentral gyrus, left middle frontal gyrus, left superior frontal gyrus, bilateral thalamus, bilateral caudate, right insula, left postcentral gyrus, bilateral lingual gyrus, bilateral parahippocampal gyrus, right superior temporal gyrus, left angular gyrus, left superior occipital gyrus, left precuneus, left middle temporal gyrus, left posterior cingulate cortex (PCC), and left cerebellum (Table 2,

Table 2. Talairach coordinates and Broadmann's areas for regions of statistically significant activation ($p<0.0005$ at voxel level uncorrected threshold) in response to virtual LBP stimulation (task – control condition).

Anatomical region	Side	Coordinate	Broadmann area	Z score
LBP group as compared to non-LBP group				
Fusiform gyrus	Lt	−46, −34, −13	Area 20	4.53
Inferior temporal gyrus	Lt	−57, −43, −15	Area 37	3.60
Precentral gyrus	Lt	−32, 8, 38	Area 9	4.38
	Rt	28, −24, 56	Area 4	4.03
Middle frontal gyrus	Lt	−46, 20, 43	Area 8	3.68
		−32, 11, 60	Area 6	3.50
Superior frontal gyrus	Lt	−40, 16, 53	Area 8	3.56
Thalamus	Lt	−24, −25, 7	-	4.34
	Rt	24, −27, 0	-	3.40
Caudate	Lt	−28, −32, 13	-	3.57
	Rt	38, −35, −3	-	3.91
Insula	Rt	28, −27, 12	Area 13	4.30
	Rt	34, −20, 18	Area 13	3.50
Postcentral gyrus	Lt	−8, −55, 64	Area 7	4.07
Lingual gyrus	Rt	18, −62, 0	Area 19	3.99
	Lt	−6, −72, −5	Area 18	3.81
Parahippocampal gyrus	Lt	−36, −43, 0	Area 19	3.96
	Rt	32, −53, −4	Area 19	3.91
	Rt	28, −41, −10	Area 36	3.62
Superior temporal gyrus	Rt	40, −35, 4	Area 41	3.78
Angular gyrus	Lt	−32, −74, 30	Area 39	3.88
Superior occipital gyrus	Lt	−38, −80, 33	Area 19	3.78
Precuneus	Lt	−42, −72, 35	Area 19	3.42
Middle temporal gyrus	Lt	−60, −35, −5	Area 21	3.62
Posterior cingulate gyrus	Lt	−10, −41, 30	Area 31	3.61
	Lt	−4, −43, 37	Area 31	3.55
Cerebellum	Lt	−24, −30, −20	-	3.88
non-LBP group as compared to LBP group				
Caudate	Rt	22, −34, 20	-	3.61

doi:10.1371/journal.pone.0026681.t002

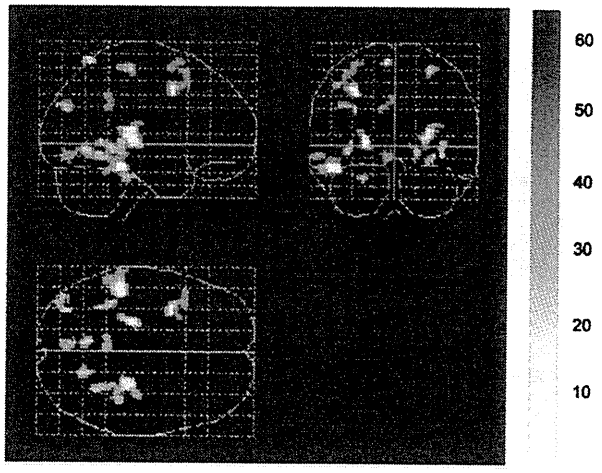

Figure 1. Areas of cortical activation in the LBP group compared with the non-LBP group in response to virtual LBP stimuli (task – control condition) detected by fMRI($p<0.0005$, Z score>3.4, uncorrected threshold).
doi:10.1371/journal.pone.0026681.g001

Fig. 1). The reverse contrast showed that the LBP group had lower activations than the non-LBP group in a single cluster in right caudate (Table 2).

In the LBP group, activations related to discomfort were found in the bilateral thalamus, bilateral medial frontal gyrus, right claustrum, left cerebellum (Table 3, Fig. 2). Activations associated with self-reported pain were found in the right thalamus and right lingual gyrus. RDQ scores were associated with activation in the left ACC, and ODI scores were associated with activations in the right insula (Table 3, Fig. 3).

Table 3. Cortial areas showing a linear signal increase with the discomfort rating, pain rating, RDQ scores and ODI scores.

Anatomical region	Side	Coordinate	Broadmann area	Z score
Discomfort				
Thalamus	Rt	20, −23, 5	-	4.19
	Lt	−4, −17, 3	-	3.78
Medial frontal gyrus	Rt	10, −22, 58	Area 6	3.85
	Lt	−12, −28, 53	Area 6	3.70
	Lt	−50, 1, 28	Area 6	3.38
Claustrum	Rt	30, 3, 13	-	3.75
Cerebellum	Lt	0, −53, −6	-	3.57
Pain				
Thalamus	Rt	20, −31, 7	-	4.27
Lingual gyrus	Rt	8, −86, −11	Area 18	3.62
RDQ				
Anterior cingulate gyrus	Lt	−6, 9, 27	Area 24	3.99
ODI				
Insula	Rt	40, −8, −5	Area 13	3.67

RDQ, Roland-Morris Disability Questionaire; ODI, Oswestry Disability Index 2.0.
doi:10.1371/journal.pone.0026681.t003

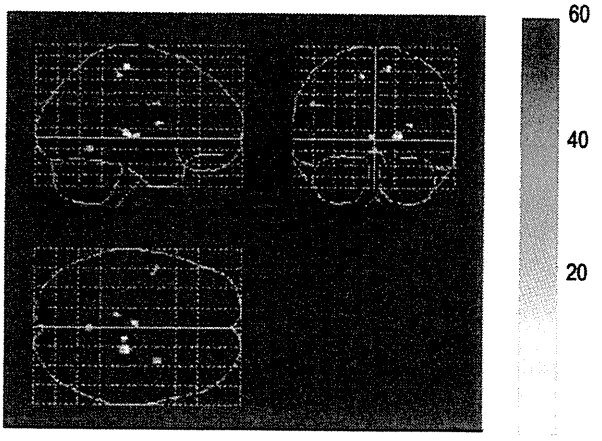

Figure 2. Areas of cortical activation showing an association with perceived discomfort.
doi:10.1371/journal.pone.0026681.g002

Discussion

Our results demonstrate that viewing images of simulated back pain evoke unpleasant feelings, and specific brain activations in individuals with LBP. According to the International Association for the Study of Pain, pain is defined as, "an unpleasant sensory and emotional experience associated with actual or potential tissue damage, or described in terms of such damage". As this definition suggests, both real pain stimuli and virtual pain experiences such as the visual stimuli in our study may play an important role in pain recognition and interpretation in the brain.

Functional MRI results showed that many of the areas described as being part of the "pain matrix" are also active during virtual pain. These results suggest that previous experiences of low back pain can sensitize an individual to pain anticipation. Activation in the insular cortex is associated with pain discrimination [17,18,19]. Additionally, the posterior insular cortex also plays a role in directing appropriate motor behaviors [20]. Furthermore, the insular cortex has projections to the SMA [21,22]. The SMA and PMA are commonly activated by pain [19,23], and usually associated with motor preparation. Activation in those areas might be associated with preparation for protective behavior against pain. In addition, we found virtual LBP stimuli led to increased activation in cerebellum. Activity in the cerebellum is frequently found in pain neuroimaging studies. Cerebellar activation is considered to be primarily associated with motor responses [13]. The need for temporally precise information may also be relevant for brain areas involved in initiating, propagating, and executing defensive motor responses to noxious stimuli [11,13,24,25].

The thalamus and the pulvinar are heavily interconnected with the visual and parietal cortices. Neuroimaging studies suggest responses in the pulvinar have a spatiotopic organization that are modulated by visual attention [26,27,28]. These results suggest that low back pain experiences may make individuals pay more attention to pain-related visual stimuli.

Many reports identify a role of the PCC in negative emotion [29,30,31,32,33,34], visuospatial orientation, and assessment of self-relevant sensation [35]. Exaggerated cerebral activation by pain stimuli may also be associated with pathologic pain states such as allodynia [36,37]. Together with its possible role in inflammatory pain [38], PCC activation could possibly reflect the negative emotion and the pathologic state of pain.

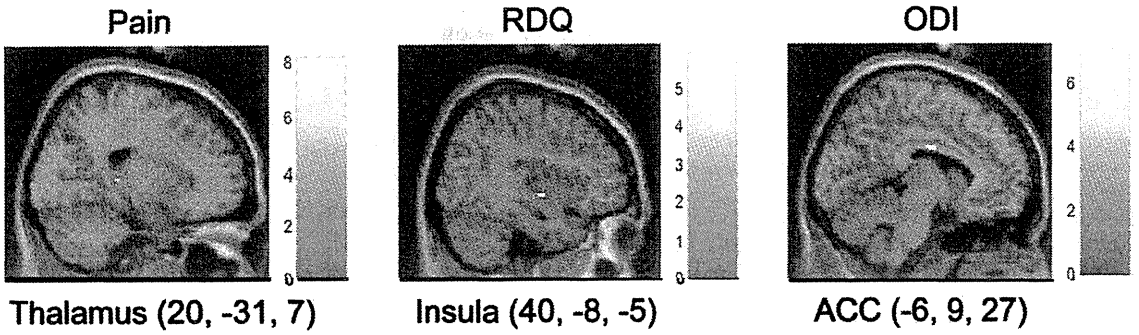

Figure 3. Sagittal sections showing cortical clusters where activity was linearly correlated with perceived pain, RDQ scores and ODI scores.
doi:10.1371/journal.pone.0026681.g003

We found other regions with heightened activity in LBP participants, in areas outside of the classic pain matrix. Those regions included the hippocampus, fusiform gyrus and angular gyrus. While not typically considered a nociceptive processing region, activation in the hippocampus has been previously reported to be activated in response to painful heat [14,39] and laser stimulation [40]. The hippocampus has been traditionally associated with recent memory consolidation [41], spatial memory [42], and fear-initiated avoidance behavior [43]. The hippocampus might also play a role in memorizing the pain stimulation and preparing fear-initiated avoidance. The fusiform gyrus is often associated with facial recognition [44]. It is conceivable, therefore, that our visual stimuli (which included a human face) may have been responsible for observed activations in the fusiform gyrus. However, our visual stimuli included a human facewithout any faical expression. This might suggest that the fusiform gyrus plays another important role in the cognitive neuroscience field. The angular gyrus is associated with empathy and 'theory of mind' [45]. Visual stimuli may cause subjects in the LBP group to imagine self pain or feel empathy towards the individual in pain in the picture.

Via parametric analyses in the LBP group, we identified several regional activations that were associated with discomfort rating, pain rating, RDQ scores and ODI scores. The SMA and PMA were related to the discomfort rating. As indicated previously, the SMA and PMA are involved in motor preparation. Activation in those areas might therefore be associated with preparation of protective behaviors against discomfort and pain. Thalamic activation was associated with both discomfort and pain ratings. Greater insula activation was associated with higher ODI scores. The thalamus and insula are considered part of the sensory component of pain processing [46]. But, a recent study suggests that imagining oneself in painful situations is sufficient to trigger some pain sensory regions [47]. The ACC was associated with RDQ scores. The ACC is an important part of affective pain processing [48,49] and can be activated in tasks of pain empathy [47,50,51,52,53,54,55]. It is unknown, therefore, whether the ACC activations, which were observed in the LBP group, were due to imagined self pain, or empathetic pain for the individual in the picture.

In this study, we showed that pain-related visual stimuli can activate several regions of the pain matrix in LBP patients, but not normal volunteers. Moreover, the pain questionnaire scores in the LBP patients were associated with greater activation of pain-processing brain regions. Functional MRI and the virtual visual tasks are non-invasive methods for probing pain-related fear and catastrophizing. These results might be applied to the evaluation of chronic pain syndromes, such as low back pain, in the future.

Materials and Methods

We recruited subjects with nonspecific LBP (LBP group) (n = 11, 6 male, 5 female, mean age 20.4 years) and subjects without LBP (non-LBP group) (n = 11, 5 male, 6 female, mean age 21.5 years). All participants were right-handed, had no history of cerebrovascular disease, and were free from any medication within 24 hours of the study. Scores for the Roland-Morris Disability Questionnaire (RDQ) and Oswestry Disability Index 2.0 (ODI) were obtained for all participants. Participants in the LBP group reported low back pain, and a RDQ or ODI score greater than zero. Participants in the non-LBP group had never experienced low back pain lasting longer than 1 week, and their RDQ and ODI scores were zero. No participants in either group displayed any evidence of structural abnormality in the lumbar spine on MRI, or any neurologic symptoms. None reported having a history of psychiatric disorders, or currently using any psychoactive medications.

We used virtual LBP stimuli depicting a man who is carrying luggage in a half-crouching position (Fig. 4). This picture represents an action that would likely cause pain in an individual with low back pain, and may therefore cause pain anticipation in the LBP group. Participants were also shown a picture depicting a man standing in front of luggage, providing the baseline stimulation (control condition) (Fig. 4). Participants in the LBP group had painful experiences in the half-crouching posture but did not have any pain in the standing posture. In addition, the participants in the LBP group currently feel little pain in daily life. During the fMRI session, trials were presented in a fixed block design. The distance between the participants' eyes and the screen was 12.5 cm, with a visual angle of 7.4×11.3°. The trials were applied eight times in each series, with each trial presentation lasting 3 seconds. The entire functional experiment lasted 150 seconds (see details of the experimental paradigm in Fig. 4). Self-reported discomfort and pain measures were collected using a numerical rating scale after the experimental session.

Images of the entire brain were acquired using GE SIGNA 3.0 Tesla scanner. Blood oxygenation level-dependent (BOLD) signals were collected with a T2-weighted, multi-slice, gradient echo-planar imaging (EPI) sequence (TE = 35 ms, TR = 3000 ms, flip angle = 90°, slice width = 4 mm, gap = 0 mm, 36 axial slices). Participants were scanned in the supine position, with the head

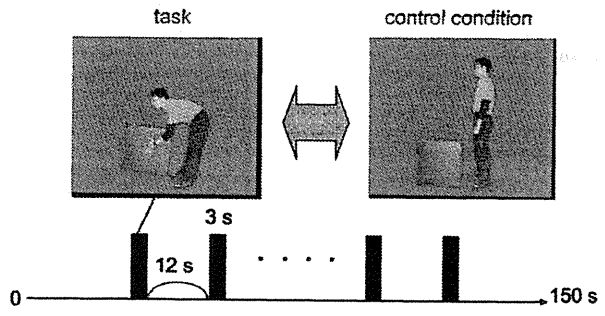

Figure 4. Experimental design. Subjects enrolled in the experiment were shown a picture demonstrating a man holding luggage in a half-crouching position (task picture) and a picture demonstrating a man standing in front of luggage, providing the baseline stimulation (control condition picture).
doi:10.1371/journal.pone.0026681.g004

fixed to minimize movement artifact. During the experiment, participants were simply instructed to observe the picture on screen.

The study was approved by the Ethical Committee of Kochi Medical School. All participants were informed of the study purpose beforehand and provided written consent to participate.

Results were analyzed on a Unix workstation using SPM2 (Statistical Parametric Mapping) software; Wellcome Department of Cognitive Neurology, Institute of Neurology, London: http://www.fil.ion.ucl.ac.uk/spm). The acquired images were realigned, spatially normalized to a standard EPI template and finally smoothed with an isotropic Gaussian kernel of 6 mm FWHM (full width at half maximum). Significance was assessed using the box car approach, convolved with the canonical hemodynamic response function. Activation maps represent t-test contrasts between the different experimental conditions. To identify the neural substrates for the virtual pain task, we contrasted the task condition and control condition in the LBP and non-LBP groups. Thresholds for activation were set at $p<0.0005$ for the voxel level of activation, and were further corrected for multiple comparisons at the cluster extent threshold of $p<0.05$. The Talairach atlas was used to anatomically localize foci of significant activation [56]. Brain activation between the LBP group and the non-LBP group was statistically compared to identify the neural processing specific to the LBP group ($p<0.05$, corrected, one-way ANOVA).

For the LBP group only, parametric analyses were also performed to determine associations between brain activity and perceived discomfort, perceived pain, RDQ score and ODI score. Normalized ratings were introduced at the subject level, taking into account only trials from the LBP group.

Acknowledgments

We would like to thank Mr. Kazuo Morio and Mr. Shin Yaogawa for technical assistance. We are grateful to KMS-TT group for the contributions of general research assistance.

Author Contributions

Conceived and designed the experiments: KS T. Ushida. Performed the experiments: KS T. Ushida. Analyzed the data: KS T. Ueno JY MN SI T. Ushida. Contributed reagents/materials/analysis tools: TI ST. Wrote the paper: KS T. Ueno JY T. Ushida.

References

1. Sullivan MJ, Rodgers WM, Kirsch I (2001) Catastrophizing, depression and expectancies for pain and emotional distress. Pain 91: 147–154.
2. Sullivan MJ, Lynch ME, Clark AJ (2005) Dimensions of catastrophic thinking associated with pain experience and disability in patients with neuropathic pain conditions. Pain 113: 310–315.
3. Van Damme S, Crombez G, Eccleston C (2004) Disengagement from pain: the role of catastrophic thinking about pain. Pain 107: 70–76.
4. Apkarian AV, Darbar A, Krauss BR, Gelnar PA, Szeverenyi NM (1999) Differentiating cortical areas related to pain perception from stimulus identification: temporal analysis of fMRI activity. J Neurophysiol 81: 2956–2963.
5. Qiu Y, Noguchi Y, Honda M, Nakata H, Tamura Y, et al. (2006) Brain processing of the signals ascending through unmyelinated C fibers in humans: an event-related functional magnetic resonance imaging study. Cereb Cortex 16: 1289–1295.
6. Wager TD, Rilling JK, Smith EE, Sokolik A, Casey KL, et al. (2004) Placebo-induced changes in FMRI in the anticipation and experience of pain. Science 303: 1162–1167.
7. Koyama T, McHaffie JG, Laurienti PJ, Coghill RC (2005) The subjective experience of pain: where expectations become reality. Proc Natl Acad Sci U S A 102: 12950–12955.
8. Ogino Y, Nemoto H, Inui K, Saito S, Kakigi R, et al. (2007) Inner experience of pain: imagination of pain while viewing images showing painful events forms subjective pain representation in human brain. Cereb Cortex 17: 1139–1146.
9. Ushida T, Ikemoto T, Tanaka S, Shinozaki J, Taniguchi S, et al. (2008) Virtual needle pain stimuli activates cortical representation of emotions in normal volunteers. Neurosci Lett 439: 7–12.
10. Ushida T, Ikemoto T, Taniguchi S, Ishida K, Murata Y, et al. (2005) Virtual pain stimulation of allodynia patients activates cortical representation of pain and emotions: a functional MRI study. Brain Topogr 18: 27–35.
11. Gracely RH, Geisser ME, Giesecke T, Grant MA, Petzke F, et al. (2004) Pain catastrophizing and neural responses to pain among persons with fibromyalgia. Brain 127: 835–843.
12. Bornhovd K, Quante M, Glauche V, Bromm B, Weiller C, et al. (2002) Painful stimuli evoke different stimulus-response functions in the amygdala, prefrontal, insula and somatosensory cortex: a single-trial fMRI study. Brain 125: 1326–1336.
13. Buchel C, Bornhovd K, Quante M, Glauche V, Bromm B, et al. (2002) Dissociable neural responses related to pain intensity, stimulus intensity, and stimulus awareness within the anterior cingulate cortex: a parametric single-trial laser functional magnetic resonance imaging study. J Neurosci 22: 970–976.
14. Derbyshire SW, Jones AK, Gyulai F, Clark S, Townsend D, et al. (1997) Pain processing during three levels of noxious stimulation produces differential patterns of central activity. Pain 73: 431–445.
15. Valet M, Sprenger T, Boecker H, Willoch F, Rummeny E, et al. (2004) Distraction modulates connectivity of the cingulo-frontal cortex and the midbrain during pain–an fMRI analysis. Pain 109: 399–408.
16. Kobayashi Y, Kurata J, Sekiguchi M, Kokubun M, Akaishizawa T, et al. (2009) Augmented cerebral activation by lumbar mechanical stimulus in chronic low back pain patients: an FMRI study. Spine (Phila Pa 1976) 34: 2431–2436.
17. Henderson LA, Gandevia SC, Macefield VG (2007) Somatotopic organization of the processing of muscle and cutaneous pain in the left and right insula cortex: a single-trial fMRI study. Pain 128: 20–30.
18. Korotkov A, Ljubisavljevic M, Thunberg J, Kataeva G, Roudas M, et al. (2002) Changes in human regional cerebral blood flow following hypertonic saline induced experimental muscle pain: a positron emission tomography study. Neurosci Lett 335: 119–123.
19. Svensson P, Minoshima S, Beydoun A, Morrow TJ, Casey KL (1997) Cerebral processing of acute skin and muscle pain in humans. J Neurophysiol 78: 450–460.
20. Berthier M, Starkstein S, Leiguarda R (1988) Asymbolia for pain: a sensory-limbic disconnection syndrome. Ann Neurol 24: 41–49.
21. Augustine JR (1996) Circuitry and functional aspects of the insular lobe in primates including humans. Brain Res Brain Res Rev 22: 229–244.
22. Luppino G, Matelli M, Camarda R, Rizzolatti G (1993) Corticocortical connections of area F3 (SMA-proper) and area F6 (pre-SMA) in the macaque monkey. J Comp Neurol 338: 114–140.
23. Hsieh JC, Stahle-Backdahl M, Hagermark O, Stone-Elander S, Rosenquist G, et al. (1996) Traumatic nociceptive pain activates the hypothalamus and the periaqueductal gray: a positron emission tomography study. Pain 64: 303–314.
24. Peyron R, Kupers R, Jehl JL, Garcia-Larrea L, Convers P, et al. (2007) Central representation of the RIII flexion reflex associated with overt motor reaction: an fMRI study. Neurophysiol Clin 37: 249–259.
25. Sullivan MJ, Thorn B, Haythornthwaite JA, Keefe F, Martin M, et al. (2001) Theoretical perspectives on the relation between catastrophizing and pain. Clin J Pain 17: 52–64.
26. Cotton PL, Smith AT (2007) Contralateral visual hemifield representations in the human pulvinar nucleus. J Neurophysiol 98: 1600–1609.

27. Fischer J, Whitney D (2009) Precise discrimination of object position in the human pulvinar. Hum Brain Mapp 30: 101–111.
28. Smith AT, Cotton PL, Bruno A, Moutsiana C (2009) Dissociating vision and visual attention in the human pulvinar. J Neurophysiol 101: 917–925.
29. Benuzzi F, Lui F, Duzzi D, Nichelli PF, Porro CA (2008) Does it look painful or disgusting? Ask your parietal and cingulate cortex. J Neurosci 28: 923–931.
30. Britton JC, Phan KL, Taylor SF, Welsh RC, Berridge KC, et al. (2006) Neural correlates of social and nonsocial emotions: An fMRI study. Neuroimage 31: 397–409.
31. Maddock RJ, Garrett AS, Buonocore MH (2003) Posterior cingulate cortex activation by emotional words: fMRI evidence from a valence decision task. Hum Brain Mapp 18: 30–41.
32. Mantani T, Okamoto Y, Shirao N, Okada G, Yamawaki S (2005) Reduced activation of posterior cingulate cortex during imagery in subjects with high degrees of alexithymia: a functional magnetic resonance imaging study. Biol Psychiatry 57: 982–990.
33. Sander K, Frome Y, Scheich H (2007) FMRI activations of amygdala, cingulate cortex, and auditory cortex by infant laughing and crying. Hum Brain Mapp 28: 1007–1022.
34. Sinha R, Lacadie C, Skudlarski P, Wexler BE (2004) Neural circuits underlying emotional distress in humans. Ann N Y Acad Sci 1032: 254–257.
35. Vogt BA (2005) Pain and emotion interactions in subregions of the cingulate gyrus. Nat Rev Neurosci 6: 533–544.
36. Freund W, Wunderlich AP, Stuber G, Mayer F, Steffen P, et al. (2010) Different activation of opercular and posterior cingulate cortex (PCC) in patients with complex regional pain syndrome (CRPS I) compared with healthy controls during perception of electrically induced pain: a functional MRI study. Clin J Pain 26: 339–347.
37. Lorenz J, Cross DJ, Minoshima S, Morrow TJ, Paulson PE, et al. (2002) A unique representation of heat allodynia in the human brain. Neuron 35: 383–393.
38. Ruehle BS, Handwerker HO, Lennerz JK, Ringler R, Forster C (2006) Brain activation during input from mechanoinsensitive versus polymodal C-nociceptors. J Neurosci 26: 5492–5499.
39. Ploghaus A, Narain C, Beckmann CF, Clare S, Bantick S, et al. (2001) Exacerbation of pain by anxiety is associated with activity in a hippocampal network. J Neurosci 21: 9896–9903.
40. Bingel U, Quante M, Knab R, Bromm B, Weiller C, et al. (2002) Subcortical structures involved in pain processing: evidence from single-trial fMRI. Pain 99: 313–321.
41. Alvarez P, Squire LR (1994) Memory consolidation and the medial temporal lobe: a simple network model. Proc Natl Acad Sci U S A 91: 7041–7045.
42. Clark RE, Broadbent NJ, Squire LR (2007) The hippocampus and spatial memory: findings with a novel modification of the water maze. J Neurosci 27: 6647–6654.
43. Hollup SA, Kjelstrup KG, Hoff J, Moser MB, Moser EI (2001) Impaired recognition of the goal location during spatial navigation in rats with hippocampal lesions. J Neurosci 21: 4505–4513.
44. Radua J, Phillips ML, Russell T, Lawrence N, Marshall N, et al. (2010) Neural response to specific components of fearful faces in healthy and schizophrenic adults. Neuroimage 49: 939–946.
45. Vollm BA, Taylor AN, Richardson P, Corcoran R, Stirling J, et al. (2006) Neuronal correlates of theory of mind and empathy: a functional magnetic resonance imaging study in a nonverbal task. Neuroimage 29: 90–98.
46. Bushnell MC, Duncan GH, Hofbauer RK, Ha B, Chen JI, et al. (1999) Pain perception: is there a role for primary somatosensory cortex? Proc Natl Acad Sci U S A 96: 7705–7709.
47. Jackson PL, Brunet E, Meltzoff AN, Decety J (2006) Empathy examined through the neural mechanisms involved in imagining how I feel versus how you feel pain. Neuropsychologia 44: 752–761.
48. Apkarian AV, Bushnell MC, Treede RD, Zubieta JK (2005) Human brain mechanisms of pain perception and regulation in health and disease. Eur J Pain 9: 463–484.
49. Davis KD, Taylor KS, Hutchison WD, Dostrovsky JO, McAndrews MP, et al. (2005) Human anterior cingulate cortex neurons encode cognitive and emotional demands. J Neurosci 25: 8402–8406.
50. Botvinick M, Jha AP, Bylsma LM, Fabian SA, Solomon PE, et al. (2005) Viewing facial expressions of pain engages cortical areas involved in the direct experience of pain. Neuroimage 25: 312–319.
51. Gu X, Han S (2007) Attention and reality constraints on the neural processes of empathy for pain. Neuroimage 36: 256–267.
52. Jackson PL, Meltzoff AN, Decety J (2005) How do we perceive the pain of others? A window into the neural processes involved in empathy. Neuroimage 24: 771–779.
53. Lamm C, Batson CD, Decety J (2007) The neural substrate of human empathy: effects of perspective-taking and cognitive appraisal. J Cogn Neurosci 19: 42–58.
54. Morrison I, Lloyd D, di Pellegrino G, Roberts N (2004) Vicarious responses to pain in anterior cingulate cortex: is empathy a multisensory issue? Cogn Affect Behav Neurosci 4: 270–278.
55. Singer T, Seymour B, O'Doherty J, Kaube H, Dolan RJ, et al. (2004) Empathy for pain involves the affective but not sensory components of pain. Science 303: 1157–1162.
56. Talairach J, Tournoux P (1988) Co-planar Stereotaxic Atlas of the Human Brain. New York: Thime Medical Publishers. 122 p.

Spine

SPINE Volume 36, Number 17, pp 1350–1358

BASIC SCIENCE

Tumor Necrosis Factor-α Antagonist Reduces Apoptosis of Neurons and Oligodendroglia in Rat Spinal Cord Injury

Ke-Bing Chen, MD,*† Kenzo Uchida, MD, PhD,* Hideaki Nakajima, MD, PhD,* Takafumi Yayama, MD, PhD,* Takayuki Hirai, MD,* Shuji Watanabe, MD,* Alexander Rodriguez Guerrero, MD,*‡ Shigeru Kobayashi, MD, PhD,* Wei-Ying Ma, MD,*†§ Shao-Yu Liu, MD, PhD,† and Hisatoshi Baba, MD, PhD*

Study Design. To examine the effects of a tumor necrosis factor (TNF)-α antagonist (etanercept) on rat spinal cord injury and identify a possible mechanism for its action.

Objective. To elucidate the contribution of etanercept to the pathologic cascade in spinal cord injury and its possible suppression of neuronal and oligodendroglial apoptosis.

Summary of Background Data. Etanercept has been recently used successfully for treatment of inflammatory disorders. However, only a few studies have examined its role in suppressing neuronal and oligodendroglial apoptosis in spinal cord injury.

Methods. Etanercept or saline (control) was administered by intraperitoneal injection 1 hour after thoracic spinal cord injury in rats. The expressions and localizations of TNF-α, TNF receptor 1 (TNFR1), and TNF receptor 2 (TNFR2) were examined by immunoblot and immunohistochemical analyses. Spinal cord tissue damage between saline- and etanercept-treated groups was also compared after hematoxylin-eosin and luxol fast blue (LFB) staining. The Basso-Beattie-Bresnahan (BBB) scale was used to evaluate rat locomotor function after etanercept administration. Terminal deoxynucleotidyl transferase (TdT)-mediated dUTP-biotin nick end labeling (TUNEL)-positive cells were counted and the immunoreactivity to active caspase-3 and caspase-8 was examined after etanercept administration.

Results. Immunoblot and double immunofluorescence staining revealed suppression of TNF-α, TNFR1, and TNFR2 expression after administration of etanercept in the acute phase of spinal cord injury. LFB staining demonstrated potential myelination in the etanercept-treated group from 2 week after spinal cord injury, together with an increased BBB locomotor score. Double immunofluorescence staining showed a significant decrease in TUNEL-positive neurons and oligodendroglia from 12 hour to 1 week in the gray and white matters after etanercept administration. Immunoblot analysis demonstrated overexpression of activated caspase-3 and caspase-8 after spinal cord injury, which was markedly inhibited by etanercept.

Conclusion. Our results indicated that etanercept reduces the associated tissue damage of spinal cord injury, improves hindlimb locomotor function, and facilitates myelin regeneration. This positive effect of etanercept on spinal cord injury is probably attributable to the suppression of TNF-α, TNFR1, TNFR2, and activated caspase-3 and caspase-8 overexpressions, and the inhibition of neuronal and oligodendroglial apoptosis.

Key words: apoptosis, neurons, oligodendroglia, spinal cord injury, tumor necrosis factor (TNF)-alpha, etanercept. **Spine 2011; 36:1350–1358**

Traumatic spinal cord injury initiates a complex series of cellular and molecular events that induce massive cell death of neurons and glial cells, extensive demyelination, and axonal destruction, leading to permanent neurologic deficits. Several studies demonstrated the rapid appearance of apoptotic neurons and glial cells in injured cord segments and adjacent areas after spinal cord injury.[1–4] Programmed cell death of oligodendroglia was also observed along the longitudinal axis of the spinal cord, possibly contributing to the delayed and prolonged demyelination process that leads to deterioration of spinal cord sensorimotor function.[3,5] Prevention of apoptosis after spinal cord injury could therefore potentially lead to spinal cord tissue repair and improved motor function. Indeed, a number of experiments have attempted to suppress apoptotic cell death after spinal cord injury.[6–8]

From the *Department of Orthopaedics and Rehabilitation Medicine, Faculty of Medical Sciences, University of Fukui, Japan; †Department of Spinal Surgery, The First Affiliated Hospital, Sun Yat-Sen University, People's Republic of China; ‡Servicio de Neurocirugia, Hospital Nacional Rosales, Universidad de El Salvador, San Salvador, El Salvador; and §Department of Anaesthesiology, The Second Affiliated Hospital, Sun Yat-Sen University, Guangzhou 510120, People's Republic of China.

Acknowledgment date: May 17, 2010. First revision date: June 22, 2010. Acceptance date: June 29, 2010.

The manuscript submitted does not contain information about medical device(s)/drug(s).

No benefits in any form have been or will be received from a commercial party related directly or indirectly to the subject of this manuscript.

Supported in part by grants-in-aid to HB, HN, and KU for General Scientific Research of the Ministry of Education, Science and Culture of Japan (grants number B18390411, B19791023, C21591895, C21791389, and B22390287).

This work was also supported by grants from the Investigation Committee on Ossification of the Spinal Ligaments (2005–2010) and Research Program for Spinal Cord Intractable Pain (2009–2010).

Address correspondence and reprint requests to Kenzo Uchida, MD, PhD, Department of Orthopaedics and Rehabilitation Medicine, Faculty of Medical Sciences, University of Fukui, Matsuoka Shimoaizuki 23-3, Eiheiji, Fukui 910-1193, Japan; E-mail: kuchida@u-fukui.ac.jp

DOI: 10.1097/BRS.0b013e3181f014ec

Tumor necrosis factor (TNF)-α is a potential trigger of neural cell injury in the spinal cord.[9–11] TNF-α mediates several biologic and immunoregulatory responses in a variety of inflammatory diseases and trauma of the central nervous system including the spinal cord.[12–15] It is highly possible that both TNF receptor 1 (TNFR1) and TNF receptor 2 (TNFR2), both members of the TNFR superfamily,[16,17] are involved in these potentially destructive cellular reactions mediated by TNF-α. In a chronic spinal cord compression model, we showed that TNF-α, TNFR1, and TNFR2 induced neuronal and oligodendroglial cell apoptosis after spinal cord injury.[18] The biologic activity of TNF-α is inhibited by the TNF-α antagonist etanercept, which has demonstrated efficacy in rheumatoid and psoriatic arthritis by reducing joint inflammation and pain.[19–21] Etanercept inhibits TNF activity by competitive binding for cell-surface receptor interactions. It binds to TNF-α and TNF-β, in a reversible fashion, and after dissociation, the TNF remains bioactive. Etanercept also reduces secondary inflammatory damage to the spinal cord after traumatic injury.[22,23] However, it remains unknown how etanercept suppresses neuronal and oligodendroglial apoptosis in spinal cord injury.

This study investigated the effects and possible mechanisms of action of etanercept in the rat spinal cord contusion model, with a particular focus on the inhibition of TNF-α-mediated neuronal and oligodendroglial apoptosis. To our knowledge, this is the first experimental investigation of etanercept on neuronal function and neurologic improvement after spinal cord injury.

MATERIALS AND METHODS

Animal Model of Spinal Cord Injury

Experiments were conducted in 108 adult male Sprague-Dawley rats (Clea, Tokyo, Japan), aged 8 to 10 weeks with a mean body weight of 275 ± 35.2 g (±SD). After anesthesia by intraperitoneal injection of sodium pentobarbiturate (0.05 mg/g body weight), laminectomy was performed at the T9 and T10 levels using a surgical microscope (VANOX-S, Olympus, Tokyo, Japan), taking utmost care to avoid damaging the dura mater. The dorsal surface of the spinal cord was compressed extradurally at the T10 cord level using a 90-g static load (custom-made rod, 2 × 3 mm in diameter) for 2 minute, as described previously.[8] In one group of rats were treated by intraperitoneal administration of etanercept at the dosage of 5 mg/kg 1 hour after the contusion (n = 45). In the other group of rats with the same magnitude of spinal cord injury (n = 45), 1 mL of saline was injected 1 hour after the contusion injury: these animals served as the control group.[23] Rats subjected to laminectomy, but with no spinal cord injury sustained, served as the sham-operated group (n = 18). After surgery, all animals were housed under a 12-hour light-dark cycle in a bacteria free biologically clean room with access to food and water *ad libitum*.

This study was carried out in the Orthopaedic Spinal Cord Laboratort of University of Fukui. The experimental protocol strictly followed the Ethics Review Committee Guidelines for Animal Experimentation of our University.

Immunoblot Analysis

Immunoblot analysis was performed at 6 hour, 12 hour, 1 day, 3 day, 1 week, and 2 week after spinal cord injury using the method described previously by our group.[8,18,24] Immediately after anesthesia by intraperitoneal injection of sodium pentobarbiturate, the damaged spinal cord around the epicenter of the lesion (longitudinal section approximately 20 mm in length) was dissected *en bloc* from the spine and stored immediately at −80°C in liquid nitrogen. Sections were centrifuged at 15,000*g* for 30 second using a BioMasher Rapid Homogenization Kit (Funakoshi Co Ltd, Tokyo, Japan). Samples were then solubilized in RIPA buffer [50 mmol/L Tris-HCl, pH 7.5, 150 mmol/L NaCl, 1% Triton X-100, 0.5% sodium deoxycholate, 20 μg/mL leupeptin, and 1 mmol/L phenylmethylsulfonylfluoride (PMSF)], homogenized, and stored at −80°C. Protein concentration was determined by a DC Protein Assay Kit (Bio-Rad Laboratories, Hercules, CA). Laemmli sodium dodecylsulfate buffer samples containing the protein mixtures were boiled and subjected to immunoblot analysis. Total protein (20 μg/lane) was separated on 12.5% SDS-PAGE and transferred onto polyvinylidene difluoride membrane (PE Applied Biosystems, Foster, CA) for 70 minute using a semidry blot apparatus. The membrane was washed twice in phosphate-buffered saline (PBS) containing 0.05% Tween 20, blocked by 5% skim milk in PBS for 1 hour at room temperature, and then incubated with either anti-TNF-α (code No. Ab9755, 1:500, rabbit IgG, Abcam plc, Cambridge, UK), anti-TNFR1 (code No. SC7895, 1:200, rabbit IgG; Santa Cruz Biotechnology, Santa Cruz, CA), anti-TNFR2 (code No. SC7862, 1:200, rabbit IgG; Santa Cruz Biotechnology), antiactive caspase-3 polyclonal antibody (code No. Ab2302, 1:200, rabbit IgG; Abcam plc), and anticaspase-8 polyclonal antibody (code No. Ab52183, 1:200, rabbit IgG; Abcam plc) overnight at 4°C, followed sequentially by antirabbit or antimouse IgG antibody and avidin-biotinylated peroxidase complex (1:10000; Envision System-HRP Labeled Polymer, Dako Cytomation, Carpenteria, CA) for 30 minutes each. After triple washing in 0.1 M PBS, the membrane was immersed in a chemiluminescence reagent for 1 minute and then subjected to radiography to visualize the peroxidase activity and thus level of antibody binding. The band intensities of TNF-α, TNFR1, TNFR2, and active-caspase-3 and caspase-8 were normalized to β-actin (code No. IMG-5142A, 1:1000, rabbit IgG, Imgenex, San Diego, CA).

Immunofluorescence Staining and Double Staining

At 6 hour, 12 hour, 1 day, 3 day, 1 week, and 2 week after spinal cord injury, animals were reanesthetized and 300 mL of PBS was perfused intracardially followed by 200 mL of 2% paraformaldehyde in 0.1 M PBS (pH 7.6). Immediately after perfusion, the spinal cord from T8–T12 cord segments was removed *en bloc* and stored in 0.1 M PBS containing 20% sucrose at 4°C for 36 hour. Tissue blocks were embedded in Tissue-Tek [optimal cutting temperature (OCT) compound 4583; Sakura Finetechnical, Tokyo, Japan), frozen, and then stored at −80°C. Three sham-operated rats that underwent laminectomy without compression were also killed

and processed for the other groups. Using a cryostat, serial 25-μm-thick transverse frozen sections were prepared for immunofluorescence staining. All sections were serially mounted on glass slides and fixed with 2% paraformaldehyde in 0.1 M PBS for 5 minutes, rinsed in PBS, and then stored at −20°C. Serial 25-μm-thick transverse frozen sections were also treated with 0.1 M Tris-HCl buffer (pH 7.6) containing 0.3% Triton-X-100 for another 24 hour to allow reaction of the cell membrane with the antibodies. Sections were incubated at 4°C overnight with anti-TNF-α antibody (code No. SC1348, 1:100, gout IgG; Santa Cruz Biotechnology), anti-TNFR1 antibody (code No. SC7895, 1:100, rabbit IgG; Santa Cruz Biotechnology), or anti-TNFR2 antibody (code No. SC7862, 1:100, rabbit IgG; Santa Cruz Biotechnology) diluted in Antibody Diluent with Background Reducing Components (Dako Cytomation, Carpinteria, CA). The secondary antibody was goat antirabbit Alexa Flour 488-conjugated antibody (1:250; Molecular Probes, Eugene, OR), applied for 1 hour at room temperature.

For double immunofluorescence staining, the sections were further incubated with antineuronal nuclei monoclonal antibody (code No. MAB377, NeuN, 1:100, mouse IgG; Chemicon International, Temecula, CA), antioligodendrocyte monoclonal antibody (code No. MAB1580, RIP, 1:100, mouse IgG; Chemicon International), antimacrophage monoclonal antibody (code No. Ab1211, OX-42, 1:100, CD11b, Abcam plc), or antiglial fibrillary acidic protein monoclonal antibody (code No. G3893, 1:100, mouse IgG; σ-Aldrich Co., St Louis, MO) diluted in Antibody Diluent with Background Reducing Components (Dako Cytomation) at 4°C overnight. The sections were then incubated with goat antimouse Alexa Flour 568-conjugated antibody (1:250; Molecular Probes). The immunostained cells were visualized under a fluorescent microscope (Olympus AX80, Tokyo, Japan) or confocal microscope equipped with a 15-mW krypton argon laser (model TCS SP2, Leica Instruments, Nussloch, Germany). The 488- and 568-nm lines of the argon/helium-neon laser were used for fluorescence excitation.

Histology and Measurement of Cystic Cavities

Sections of the spinal cord were also taken at the same earlier-mentioned time course of immunohistochemistry after intracardial perfusion with PBS and 4% paraformaldehyde. Sections were fixed for 24 hour in 4% paraformaldehyde solution at 4°C, dehydrated through a graded ethanol series, and embedded in paraffin. Tissue sections (10-μm thick) were deparaffinized in xylene and stained with luxol fast blue (LFB) and with hematoxylin and eosin (HE). For a semiquantitative analysis of demyelination, lesion areas were cross-referenced with the HE staining to establish cellularity. The axial 10 random sections within 1500 μm rostral and caudal to the epicenter were examined using standard brightfield microscopy. At 2 week, 4 week, and 8 week after spinal cord injury, LFB-positive areas in ventrolateral funiculus were analyzed under 400× magnification using grain counting with the light intensity automatically set by a color image analyzer (MacSCOPE; Mitani, Fukui, Japan). LFB-positive area in which the density significantly exceeded the threshold of each background was calculated as percentage cross-sectional area of residual tissue.[25]

Assessment of Locomotor Behavior

To assess the behavior of each rat after spinal contusion and recovery of locomotor function, 48 rats from each group [the control (injected with saline), etanercept-treated, and sham-operated groups] were investigated at 1 day, 3 day, 1 week, 2 week, 4 week, and 8 week after administration of saline or etanercept. Locomotor function of the hind limbs was graded using the Basso-Beattie-Bresnahan (BBB) hind limb locomotor rating scale.[26] The BBB rating scale is a 21-point system on the basis of operationally defined behavioral features, which follow the recovery progression from complete paralysis to normal locomotion. The rating scale ranges from 0 to 21, with a score of 0 indicating complete hind limb paralysis, whereas a score of 21 denotes completely normal locomotor function. Scores of 0 to 20 indicate an animal's altered ability to move the hind limb joints, to bear weight, and to coordinate forelimb and hind limb movement.

Terminal Deoxynucleotidyl Transferase (TdT)-Mediated dUTP-Biotin Nick End Labeling (TUNEL) Staining

Serial 25-μm-thick transverse frozen sections were prepared for TUNEL staining as for immunofluorescence staining. Deoxyribonucleic acid fragmentation was detected by the TUNEL method using the ApopTag Peroxidase *in situ* Apoptosis Detection kit (Chemicon International). The experiments were performed as described in the kit manual. The reaction with TdT was terminated by washing the sections with stop-wash buffer for 10 minute at room temperature. Antidigoxigenin peroxidase was then applied for 30 minute at room temperature, and then the sections were incubated with antineuronal nuclei monoclonal antibody (code No. MAB377, NeuN, 1:100, mouse IgG; Chemicon International) and antioligodendrocyte monoclonal antibody (code No. MAB1580, RIP, 1: 100, mouse IgG; Chemicon International) diluted in Antibody Diluent with Background Reducing Components at 4°C overnight. Goat antimouse Alexa Flour 568/fluorescein-conjugated secondary antibody (1: 250; Molecular Probes) was subsequently applied. To quantitatively examine the numbers of apoptotic cells, TUNEL-positive cells at each time point were counted in 20 random sections between 5 mm and 10 mm rostral and caudal to the injury epicenter, respectively on gray matter and white matter of sections from control and etanercept-treated animals with a color image analyzer (MacSCOPE). The average number of sections labeled with TUNEL (green) was calculated throughout the lesion site of each animal. The number of TUNEL-positive cells in which the density significantly exceeded the threshold in each background calculated in sham-operated rats in each gray and white matter was counted.[27] The immunostained cells were also visualized by confocal microscopy.

Statistical Analysis

All values are expressed as mean ± SD. Differences between groups were examined for statistical significance using the

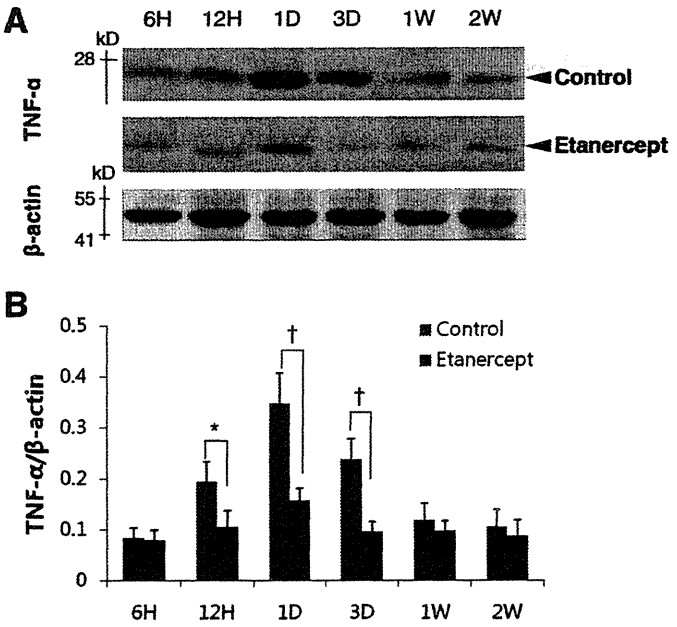

Figure 1. A, Immunoblot analysis of TNF-α expressions in saline groups (control) and etanercept-treated groups. **B**, Graphs indicate relative band intensities compared with that of β-actin. The relative expression in the etanercept-treated group was weaker than those in the control animals, especially in the acute phase (12 hours, 1 day, 3 day) after spinal cord injury compared (B: n = 3 for each time point).

paired *t* test. A $P < 0.05$ denoted the presence of a significant difference. The above tests were conducted using SPSS software version 11.0 (SPSS, Chicago, IL).

RESULTS

Temporal Pattern of Inflammatory Cytokine Expression with or Without Etanercept Administration

Differences in TNF-α expression in the injured spinal cord were assessed by immunoblot analysis with or without etanercept administration at several time points after spinal cord injury (Figure 1A). The highest expression of TNF-α was observed at 1 day after cord injury. Administration of etanercept significantly suppressed the TNF-α expression at 12 hour, 1 day, and 3 day after cord injury (Figure 1B). Next, we evaluated the cellular expression of TNF-α pathway components by double immunofluorescent staining using TNF-α/NeuN (for neurons), TNF-α/OX-42 (for macrophages), TNF-α/GFAP (for astrocytes), and TNFR1/RIP and TNFR2/RIP (for oligodendrocytes). Spinal cord injury resulted in the induction of TNF-α expression in neurons, oligodendroglia, microglia, and astroglial cells at 1 day after the cord injury (Figure 2 upper row, control) at an adjacent section of epicenter. Etanercept treatment suppressed the expression of TNF-α in all neurons and glial cells (Figure 2; lower row).

Cellular Expression of the TNF-α/TNFR Pathway in Injured Spinal Cord

Differences in expressions of TNFR1 and TNFR2 between control groups and etanercept-administered groups were investigated by immunoblot analysis (Figure 3A). Overexpression of TNFR1 and TNFR2 was evident in the injured spinal cord at 6 and 12 hour after the contusion injury in control animals, whereas in the etanercept-treated group, the immunoreactivity was decreased for TNFR1 at 6 and 12 hour and for TNFR2 at 6 hour after injury (Figure 3B, C).

Double-stained sections for TNFR1 and TNFR2 with neural and oligodendroglial cell marker revealed markedly reduced coexpression of TNFR1 and TNFR2 with NeuN in the gray matter or RIP in the white matter at 6 hour after injury in etanercept-treated animals at 5 mm rostral to the epicenter (Figure 4).

Histologic Evaluation of the Injured Spinal Cord

The severity of trauma at the injury epicenter site was evaluated in both groups. Axial samples of the spinal cord were evaluated at each time point using HE and LFB staining. HE staining (Figure 5A) showed a significant decrease in neural injury with etanercept treatment (right column panels) compared to controls; edema was also reduced and structural preservation of the spinal cord was enhanced. Cystic formation was weak in the etanercept group at 2, 4, and 8 week after injury. In LFB-stained samples, while at 2, 4, and 8 week, images demonstrated significantly smaller areas of

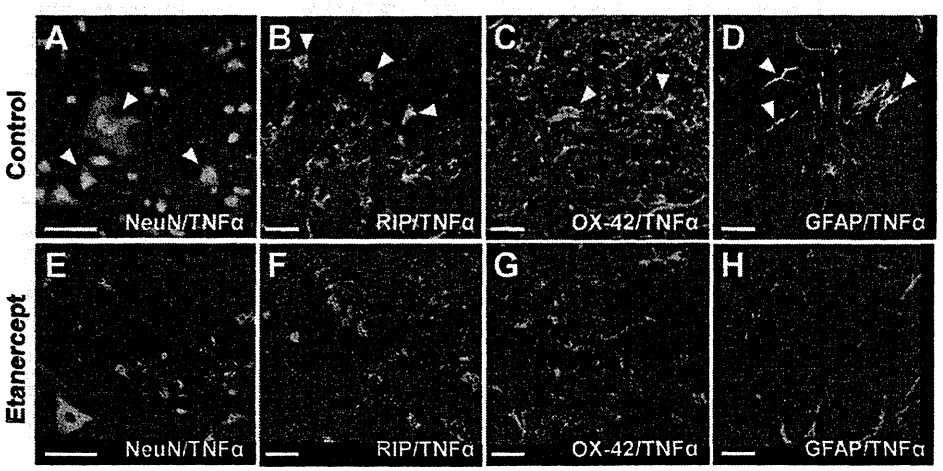

Figure 2. Photomicrograph showing the colocalization of cell-specific markers (red) and TNF-α (green) in saline groups and etanercept-administered groups at 1 day after spinal cord injury at 5 mm rostral to the injury epicenter. Expression of TNF-α was significant in neurons (NeuN: **A**), oligodendroglia (RIP: **B**), microglia (OX-42: **C**), and astroglial cells (GFAP: **D**) in control. In the etanercept-treated group (**E–H**), numbers of all double-positive cells (yellow) were significantly decreased. Arrowheads indicate colocalization of the cell-specific marker and TNF-α. Scale bar = 50 μm (**A, E**), 10 μm (**B–D, F–H**).

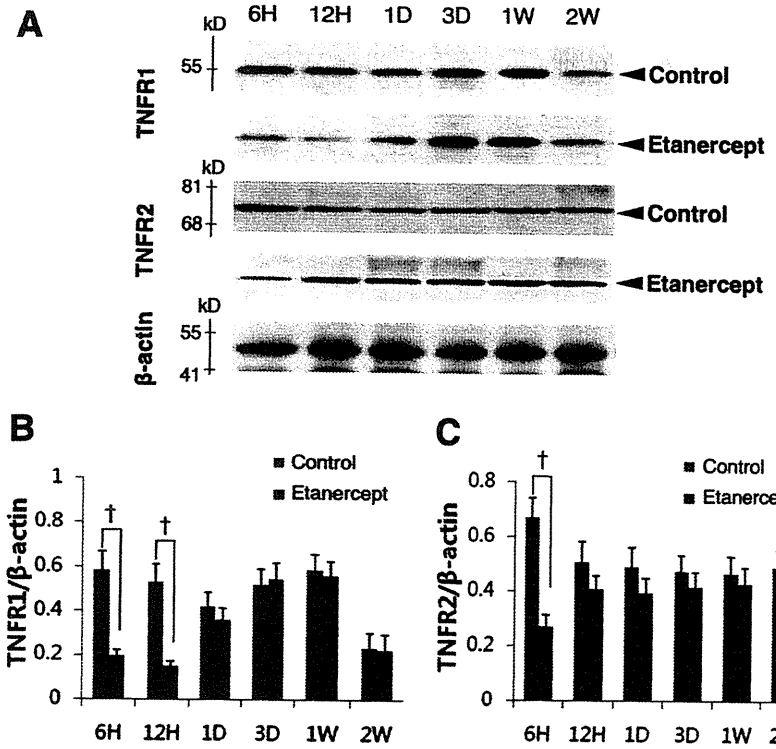

Figure 3. A, Immunoblot analysis of TNFR1 and TNFR2 expression at several time intervals after spinal cord injury. Graphs indicate relative band intensity compared with that of β-actin (**B**, **C**: n = 3 for each time point). TNFR1 expression was significantly low in the treatment group at 6- and 12-hour postinjury compared to the controls. TNFR2 expression was also reduced in the etanercept-treated group at 6 hour compared to controls. The data are expressed as mean ± SD. $*P < 0.05$, $\dagger P < 0.01$, compared to β-actin.

cystic cavity formation and enhanced staining in both gray and white matters (Figure 5B, C). At the injury epicenter sites, the percentage cross-sectional area of residual tissue was significantly larger in the etanercept-treated group than in controls at 2 week, 4 week, and 8 week after spinal cord injury (Figure 5D).

Evaluation of Locomotor BBB Score

The degree of motor disturbance in the hind limbs was assessed at 1 day, 3 day, 1 week, 2 week, 4 week, and 8 week after spinal cord injury. Rats sustaining spinal cord injury had significant motor disturbances in the hind limb. Etanercept administration significantly increased the BBB locomotor score at 2, 4, and 8 week after the cord injury (Figure 6).

Effects of Etanercept on Neural and Glial Cell Apoptosis

Significant levels of TUNEL/NeuN and TUNEL/RIP double staining were evident in samples from the control group; whereas etanercept-treated animals showed fewer TUNEL/NeuN and TUNEL/RIP positive cells (Figure 7A, B). Counting of the TUNEL-positive cells in saline groups and etanercept-administered groups using a color image analyzer (MacSCOPE) showed significantly decreased numbers at 12 hour, 1 day, 3 day, and 1 week after the cord injury in the gray matters of etanercept-treated rats (Figure 7C), and at 12 hour, 1 day, 3 day, and 1 week in the white matters of etanercept-treated animals at the adjacent sites to the epicenter (Figure 7D).

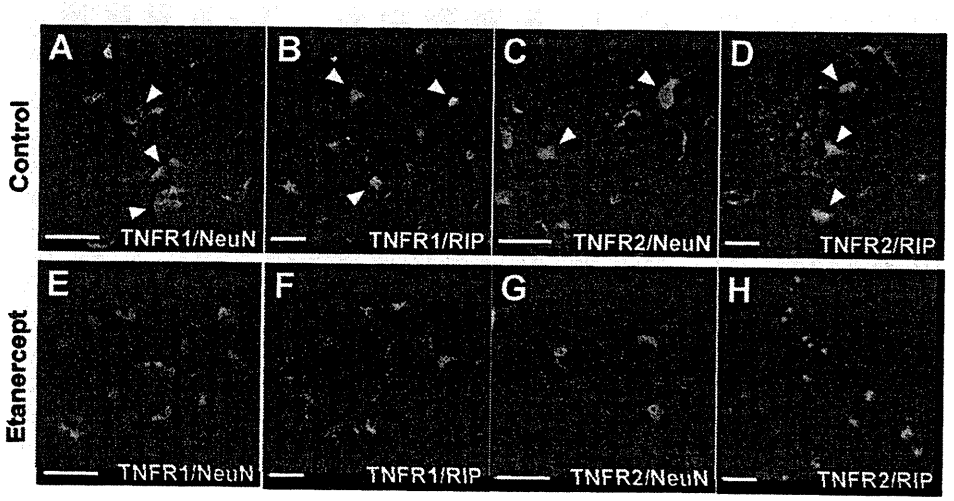

Figure 4. Photomicrograph showing colocalization of the cell marker (NeuN and RIP; red) with either TNFR1 or TNFR2 (green) in the control groups (**A–D**) and etanercept-treated (**E–H**) groups at 6 hour after spinal cord injury at 5 mm rostral to the epicenter. The expressions of both receptors on neurons in the gray matter and oligodendroglia in the white matter were markedly suppressed by etanercept administration. Arrowheads indicate colocalization (yellow) of the cell-specific marker and TNFR1 or TNFR2. Scale bar = 50 μm (**A, E**), 10 μm (**B–D, F–H**).

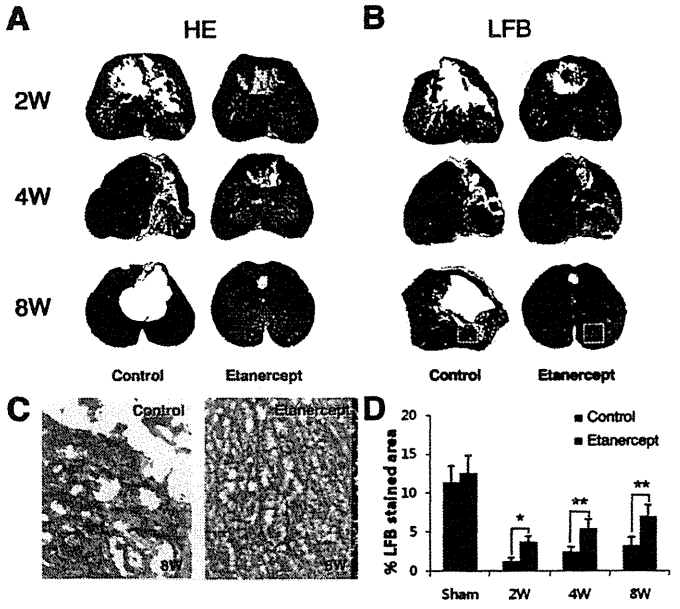

Figure 5. Histological evaluation of cord injury with HE (**A**) and LFB (**B**) staining. A, B, The etanercept group showed a lower degree of spinal cord tissue damage and edema than control groups at the injury epicenter. LFB staining of the ventral microcystic cavity at 8 week after cord injury (box area in B) showed a remarkable reduction in the area of demyelination in the etanercept-treated group compared with the control group (**C**). Percentage of cross-sectional area of residual tissue and cavitations at the injury epicenter sites represented from 2 to 8 week after spinal cord injury (**D**: n = 3 for each time point). An overall significant difference was found in the areas of residual tissue and cavitations ($P < 0.001$). The percentage cross-sectional area of residual tissue was significantly different between groups at each time point. $^*P < 0.05$, $\dagger P < 0.01$.

Next, we compared the protein expression levels of active caspase-3 and caspase-8 after etanercept administration. The band intensities for both active caspase-3 and caspase-8 in the etanercept group were relatively weaker than those in controls, particularly in the acute phase (6 hour, 12 hour, 1 day, and 3 day) after cord injury (Figure 8).

DISCUSSION

This study provided new insights on spinal cord injury by investigating the effect of TNF-α antagonist, etanercept, in the rat spinal cord injury. The main effects of etanercept demonstrated herein were as follows: (1) reduction of TNF-α, TNFR1, and TNFR2 overexpression, especially in neurons and oligodendroglia in the acute phase of spinal cord injury; (2) prevention of tissue damage and demyelination in the spinal cord 2 week after the cord injury and thereafter; (3) increase in the locomotor BBB score in the hindlimb at 2 week and thereafter after injury; and (4) suppression of neuronal and oligodendroglial cell apoptosis in both gray and white matter of the spinal cord at the adjacent sites the injury epicenter. These findings indicated that etanercept could potentially play an important role in reducing neural damage of the spinal cord after traumatic injury *via* its suppressive actions on the TNF-mediated proinflammatory response

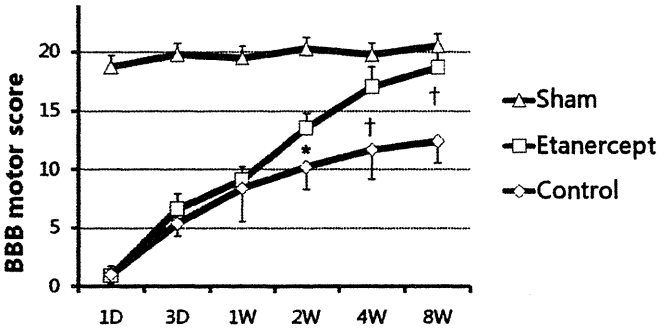

Figure 6. Analysis of locomotor BBB score after the cord injury. A significant improvement in hindlimb motor function was observed in the etanercept-treated group compared with the control groups from 2 week after the injury (n = 3 for each time point; n = 2 in sham-operated group). $^*P < 0.05$, $\dagger P < 0.01$.

and on apoptosis of neurons and oligodendroglia within the spinal cord.

The cascade of secondary tissue damage after spinal cord injury is accompanied by an inflammatory response marked

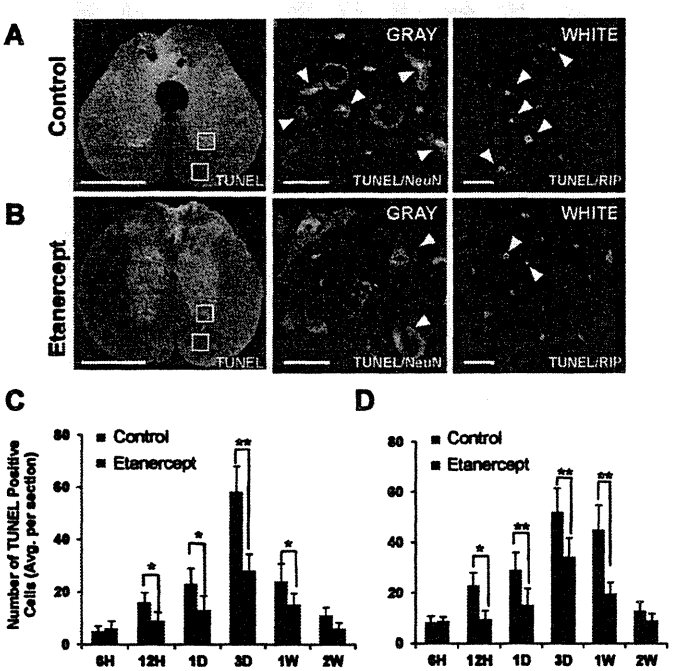

Figure 7. Representative TUNEL staining and the double immunofluorescence staining (box area in TUNEL staning) of TUNEL-positive cells (green) with NeuN or RIP (red) in control groups (**A**) and etanercept-treated (**B**) groups at 3 day after spinal cord injury at 5 mm rostral to the epicenter. Arrowheads indicate colocalization of TUNEL-positive cells and the cell-specific marker. In the etanercept-treated group (**B**), numbers of all double-positive cells (yellow) were significantly decreased. Bar graphs (**C, D**) represent the quantitative analysis of TUNEL-positive cells per cross section in the gray and white matters of both groups between 5 mm with 10 mm rostral and caudal to the injury epicenter (n = 3 for each time point). The number of TUNEL-positive neurons in the gray matter (**C**) and oligodendroglia in the white matter (**D**) was decreased in the etanercept-treated group at the adjacent site to the epicenter. Scale bars = 500 μm (left column), 50 μm (middle column), 10 μm (right column). Data are mean ± SD. $^*P < 0.05$, $\dagger P < 0.01$.

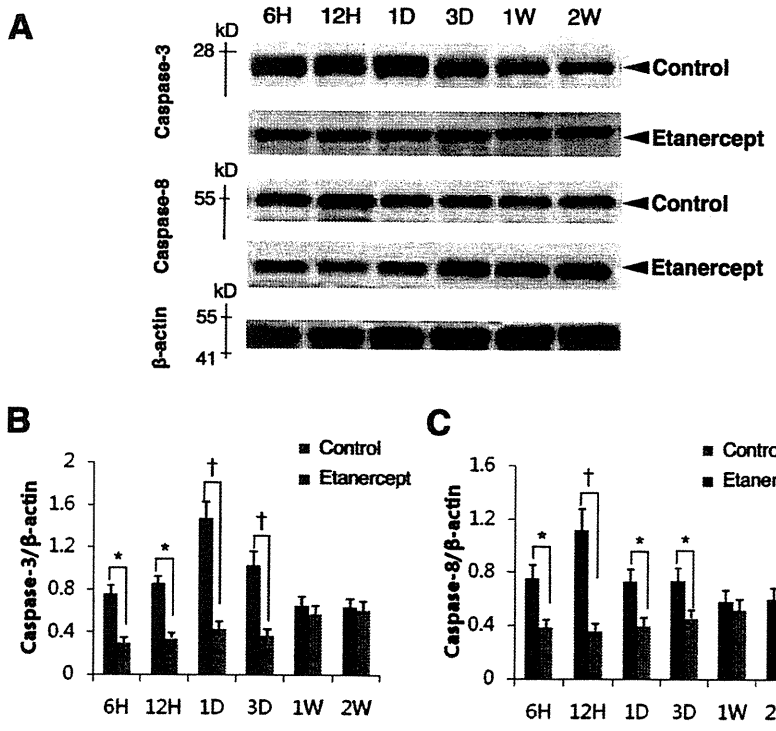

Figure 8. Immunoblot results showing expression of activated caspase-3 and caspase-8 at several time intervals after spinal cord injury (**A**). Graphs indicate relative band intensities compared with that of β-actin (**B**, **C**: n = 3 for each time point). The intensity of both activated caspase-3 and caspase-8 bands in the treatment group was significantly low at 6 hour, 12 hour, 1 day, and 3 day, compared to control animals. The data are expressed as mean ± SD. $*P < 0.05$, $\dagger P < 0.01$, compared to β-actin.

by infiltration of neutrophils and macrophages, activation of glial cells, and upregulated expression of proinflammatory cytokines.[28–30] Together, these factors lead to increased vascular permeability, edema, and degradation of the extracellular matrix. Proinflammatory cytokines including TNF-α, interleukin (IL)-1β, and IL-6 are involved in recruiting leukocytes and activating macrophages and microglia, and such cytokines are upregulated early in the inflammatory response.[31] These inflammatory cytokines, and particularly TNF-α, can initiate a large number of cellular responses including cytotoxicity, inflammation, immunoregulation, and transcriptional regulation of a large number of genes.[32] This study demonstrated that blocking the action of TNF-α decreased the magnitude of spinal cord tissue damage, reduced the extent of edema, and suppressed demyelination. Recently, Genovese *et al*[22] demonstrated that etanercept, reduced the expression of all these cytokines in a mouse model of spinal cord injury. Considered together, the present results and the above findings[22] suggest that TNF-α plays a detrimental role in the development and persistence of spinal cord injury and may in fact be one of the most important biologic triggers of the proinflammatory response in such cases.

Apoptotic neuronal and glial cells, including microglia, show overexpression of TNF-α in spinal cord injury, and it was suggested that TNF-α triggers oligodendroglial cell apoptosis, although the source of TNF-α in injured spinal cord was not identified.[33,34] A previous study also suggested that activated microglia secrete various cytotoxic factors including TNF-α in response to axonal regeneration and can therefore induce apoptosis of oligodendrocytes.[35] It was also reported that the population of apoptotic cells after spinal cord contusion injury comprises oligodendroglial cells, possibly phagocytic microglia or macrophages.[36] Double immunofluorescence staining in this study demonstrated the expression of TNF-α in not only microglia but also neurons, oligodendroglia, and reactive astroglia in the acute phase of spinal cord injury, and that etanercept seemed effective at suppressing TNF-α in all these cells. In addition, our results showed that etanercept suppressed the expression of both TNFR1 and TNFR2 in neurons and oligodendroglia.

TNF-α has been associated with degeneration of the remaining axons in the injury sites of spinal cords,[33] the promotion of myelin phagocytosis by macrophages,[37] and the death of the remaining oligodendrocytes capable of regenerating the myelin sheet. It has been considered that TNF-α eventually leads to a massive demyelination.[36] Etanercept is a dimeric fusion protein consisting of two extracellular domains of the human p75 TNF receptor, linked to the Fc portion of a type 1 human immunoglobulin (IgG1), which helps to retain the molecule in the circulation.[38] By competitive inhibition, the molecule of etanercept binds to two of the three receptor-binding sites on the TNF trimer; preventing TNF-α binding to the cell membrane receptors.[39] In this study, etanercept reduced the associated tissue damage of spinal cord injury and improved hindlimb locomotor function from 2 week after spinal cord injury. Our results may indicate that injection of etanercept after spinal cord injury leads to not only a delay of demyelination but also of the axonal degeneration at the injured site.

A variety of signal transduction pathways are involved in the complex process of apoptosis. Caspases are a family of cysteine proteases that are important in the effector phase of

apoptosis. Caspases are activated through intrinsic and extrinsic pathways. Spinal cord injury induces apoptosis *via* the activation of caspase-3[40] and increased expression of death receptors, especially Fas and p75 receptors.[41] On the contrary, the extrinsic pathway is initiated by ligands of cell-surface death receptors belonging to the TNF/nerve growth factor receptor superfamily.[42] The discovery and studies of a "death domain" in TNFR1 and related receptors revealed much about the signaling pathways mediating the activation of caspase-8 and caspase-3, before apoptosis.[43] It therefore seems reasonable to suggest that after a traumatic injury to the spinal cord, accumulation of TNF-α could initiate an apoptotic cascade *via* receptor-mediated signaling. Although TNFR1 mediates the majority of the apoptotic effects, whereas TNFR2 predominantly transmits cell-survival signals, their complete suite of locations and roles in TNF-α-induced signaling remains incomplete and controversial.[44] Holmes *et al*[17] localized the TNF receptors by immunocytochemistry; TNFR1 was found on neuronal cells and afferent fibers within the dorsal root ganglion, whereas TNFR2 immunoreactivity was absent in these locations. On the contrary, Yan *et al*[16] reported possible roles for TNFR1 and TNFR2 in adult rat spinal cord injury. These authors reported overexpression of TNFR1 and TNFR2 in the spinal cord and localized the receptors on neurons, astroglia, and oligodendroglia in spinal cord injury. Our results now indicate that suppression of both TNF-α receptors in the acute phase of spinal cord damage might inhibit apoptosis of neural and glial cells, whereas lifting the suppression of TNFR2 expression from 12 hour onward after the injury with TNF-α antagonist promoting regeneration of these same cells and contribute to a better recovery of locomotor function and decreased spinal cord tissue damage.

In conclusion, our results demonstrated that the administration of etanercept is likely to reduce the development of inflammatory tissue injury after spinal cord contusion. They also suggested that suppression of TNF-α/TNFR in the acute phase of cord injury by etanercept administration could contribute to inhibition of neuronal and glial cell apoptosis and promote better recovery of locomotor function.

➢ Key Points

- Expression of TNF-α, TNFR1, and TNFR2 in neurons and oligodendroglia in spinal cord injury could be suppressed by etanercept administration.
- Etanercept treatment induced an increased neurologic locomotor score, a decreased number of TUNEL-positive apoptotic neurons and oligodendroglia, and possibly myelination within 2 weeks after spinal cord injury.
- The current findings suggested that etanercept could improve spinal cord tissue damage, probably by suppressing TNF-α, TNFR1, TNFR2, and activated caspase-3 and caspase-8 expressions in the acute phase, and inhibiting the neuronal and oligodendroglial apoptosis caused by spinal cord injury.

References

1. Katoh K, Ikata T, Katoh S, et al. Induction and its spread of apoptosis in rat spinal cord after mechanical trauma. *Neurosci Lett* 1996;216:9–12.
2. Li GL, Brodin G, Farooque M, et al. Apoptosis and expression of Bcl-2 after compression trauma to rat spinal cord. *J Neuropathol Exp Neurol* 1996;55:280–9.
3. Crowe MJ, Bresnahan JC, Shuman SL, et al. Apoptosis and delayed degeneration after spinal cord injury in rats and monkeys. *Nat Med* 1997;3:73–6.
4. Nakahara S, Yone K, Sakou T, et al. Induction of apoptosis signal regulating kinase 1 (ASK1) after spinal cord injury in rats: possible involvement of ASK1-JNK and -p38 pathways in neuronal apoptosis. *J Neuropathol Exp Neurol* 1999;58:442–50.
5. Abe Y, Yamamoto T, Sugiyama Y, et al. Apoptotic cells associated with Wallerian degeneration after experimental spinal cord injury: a possible mechanism of oligodendroglial death. *J Neurotrauma* 1999;16:945–52.
6. Koda M, Murakami M, Ino H, et al. Brain-derived neurotrophic factor suppresses delayed apoptosis of oligodendrocytes after spinal cord injury in rats. *J Neurotrauma* 2002;19:777–85.
7. Tian DS, Xie MJ, Yu ZY, et al. Cell cycle inhibition attenuates microglia induced inflammatory response and alleviates neuronal cell death after spinal cord injury in rats. *Brain Res* 2007;1135:177–85.
8. . Nakajima H, Uchida K, Yayama T, et al. Targeted retrograde gene delivery of brain-derived neurotrophic factor suppresses apoptosis of neurons and oligodendroglia after spinal cord injury in rats. *Spine* 2010;35:497–504.
9. Yune TY, Chang MJ, Kim SJ, et al. Increased production of tumor necrosis factor-alpha induces apoptosis after traumatic spinal cord injury in rats. *J Neurotrauma* 2003;20:207–19.
10. Yune TY, Lee SM, Kim SJ, et al. Manganese superoxide dismutase induced by TNF-beta is regulated transcriptionally by NF-kappaB after spinal cord injury in rats. *J Neurotrauma* 2004;21:1778–94.
11. Profyris C, Cheema SS, Zang D, et al. Degenerative and regenerative mechanisms governing spinal cord injury. *Neurobiol Dis* 2004;15:415–36.
12. Feuerstein GZ, Liu T, Barone FC. Cytokines, inflammation, and brain injury: role of tumor necrosis factor-alpha. *Cerebrovasc Brain Metab Rev* 1994;6:341–60.
13. Arvin B, Neville LF, Barone FC, et al. The role of inflammation and cytokines in brain injury. *Neurosci Biobehav Rev* 1996;20:445–52.
14. Wang CX, Nuttin B, Heremans H, et al. Production of tumor necrosis factor in spinal cord following traumatic injury in rats. *J Neuroimmunol* 1996;69:151–6.
15. Bartholdi D, Schwab ME. Expression of pro-inflammatory cytokine and chemokine mRNA upon experimental spinal cord injury in mouse: an in situ hybridization study. *Eur J Neurosci* 1997;9:1422–38.
16. Yan P, Liu N, Kim GM, et al. Expression of the type 1 and type 2 receptors for tumor necrosis factor after traumatic spinal cord injury in adult rats. *Exp Neurol* 2003;183:286–97.
17. Holmes GM, Hebert SL, Rogers RC, et al. Immunocytochemical localization of TNF type 1 and type 2 receptors in the rat spinal cord. *Brain Res* 2004;1025:210–9.
18. Inukai T, Uchida K, Nakajima H, et al. Tumor necrosis factor-alpha and its receptors contribute to apoptosis of oligodendrocytes in the spinal cord of spinal hyperostotic mouse (twy/twy) sustaining chronic mechanical compression. *Spine* 2009;34:2848–57.
19. Moreland LW, Baumgartner SW, Schiff MH, et al. Treatment of rheumatoid arthritis with a recombinant human tumor necrosis factor receptor (p75)-Fc fusion protein. *N Engl J Med* 1997;337:141–7.
20. Seymour HE, Worsley A, Smith JM, et al. Anti-TNF agents for rheumatoid arthritis. *Br J Clin Pharmacol* 2001;51:201–8.
21. Catrina AI, Trollmo C, af Klint E, et al. Evidence that anti-tumor necrosis factor therapy with both etanercept and infliximab induces apoptosis in macrophages, but not lymphocytes, in rheumatoid arthritis joints: extended report. *Arthritis Rheum* 2005;52:61–72.
22. Genovese T, Mazzon E, Crisafulli C, et al. Immunomodulatory effects of etanercept in an experimental model of spinal cord injury. *J Pharmacol Exp Ther* 2006;316:1006–16.

23. Genovese T, Mazzon E, Crisafulli C, et al. Combination of dexamethasone and etanercept reduces secondary damage in experimental spinal cord trauma. *Neuroscience* 2007;150: 168–81.
24. Uchida K, Nakajima H, Inukai T, et al. Adenovirus-mediated retrograde transfer of neurotrophin-3 gene enhances survival of anterior horn neurons of twy/twy mice with chronic mechanical compression of the spinal cord. *J Neurosci Res* 2008;86: 1789–800.
25. Shi X, Kang Y, Hu Q, et al. A long-term observation of olfactory ensheathing cells transplantation to repair white matter and functional recovery in a focal ischemia model in rat. *Brain Res* 2010;1317:257–67.
26. Basso DM, Beattie MS, Bresnahan JC. Graded histological and locomotor outcomes after spinal cord contusion using the NYU weight-drop device versus transection. *Exp Neurol* 1996;139: 244–56.
27. Dubreuil CI, Winton MJ, McKerracher L. Rho activation patterns after spinal cord injury and the role of activated Rho in apoptosis in the central nervous system. *J Cell Biol* 2003;162:233–43.
28. Dusart I, Schwab ME. Secondary cell death and the inflammatory reaction after dorsal hemisection of the rat spinal cord. *Eur J Neurosci* 1994;6:712–24.
29. Hayashi M, Ueyama T, Nemoto K, et al. Sequential mRNA expression for immediate early genes, cytokines, and neurotrophins in spinal cord injury. *J Neurotrauma* 2000;17:203–18.
30. Pineau I, Lacroix S. Proinflammatory cytokine synthesis in the injured mouse spinal cord: multiphasic expression pattern and identification of the cell types involved. *J Comp Neurol* 2007;500: 267–85.
31. Nakamura M, Houghtling RA, MacArthur L, et al. Differences in cytokine gene expression profile between acute and secondary injury in adult rat spinal cord. *Exp Neurol* 2003;184:313–25.
32. Tartaglia LA, Ayres TM, Wong GH, et al. A novel domain within the 55 kd TNF receptor signals cell death. *Cell* 1993;74:845–53.
33. Lee YB, Yune TY, Baik SY, et al. Role of tumor necrosis factor-alpha in neuronal and glial apoptosis after spinal cord injury. *Exp Neurol* 2000;166:190–5.
34. Yune TY, Chang MJ, Kim SJ, et al. Increased production of tumor necrosis factor-alpha induces apoptosis after traumatic spinal cord injury in rats. *J Neurotrauma* 2003;20:207–19.
35. Deng Y, Lu J, Sivakumar V, et al. Amoeboid microglia in the periventricular white matter induce oligodendrocyte damage through expression of proinflammatory cytokines via MAP kinase signaling pathway in hypoxic neonatal rats. *Brain Pathol* 2008;18:387–400.
36. Shuman SL, Bresnahan JC, Beattie MS. Apoptosis of microglia and oligodendrocytes after spinal cord contusion in rats. *J Neurosci Res* 1997;50:798–808.
37. Zhang SC, Goetz BD, Carré JL, et al. Reactive microglia in dysmyelination and demyelination. *Glia* 2001;34:101–9.
38. Mohler KM, Torrance DS, Smith CA, et al. Soluble tumor necrosis factor (TNF) receptors are effective therapeutic agents in lethal endotoxemia and function simultaneously as both TNF carriers and TNF antagonists. *J Immunol* 1993;151:1548–61.
39. Spencer-Green G. Etanercept (Enbrel): update on therapeutic use. *Ann Rheum Dis* 2000;59(Suppl 1):146–9.
40. Springer JE, Azbill RD, Knapp PE. Activation of the caspase-3 apoptotic cascade in traumatic spinal cord injury. *Nat Med* 1999;5:943–6.
41. Casha S, Yu WR, Fehlings MG. Oligodendroglial apoptosis occurs along degenerating axons and is associated with FAS and p75 expression following spinal cord injury in the rat. *Neuroscience* 2001;103:203–18.
42. Ashkenazi A, Dixit VM. Death receptors: signaling and modulation. *Sci* 1998;281:1305–8.
43. Hisahara S, Shoji S, Okano H, et al. ICE/CED-3 family executes oligodendrocyte apoptosis by tumor necrosis factor. *J Neurochem* 1997;69:10–20.
44. Gupta S. A decision between life and death during TNF-alpha-induced signaling. *J Clin Immunol* 2002;22:185–94.

Uchida et al. Arthritis Research & Therapy 2011, 13:R144
http://arthritis-research.com/content/13/5/R144

arthritis research&therapy

RESEARCH ARTICLE Open Access

Ossification process involving the human thoracic ligamentum flavum: role of transcription factors

Kenzo Uchida[1†], Takafumi Yayama[1*†], Hong-Xin Cai[1,2], Hideaki Nakajima[1], Daisuke Sugita[1], Alexander Rodríguez Guerrero[1,3], Shigeru Kobayashi[1], Ai Yoshida[1], Ke-Bing Chen[1,4] and Hisatoshi Baba[1]

Abstract

Introduction: Ossification of the ligamentum flavum (OLF) of the spine is associated with serious neurologic compromise, but the pathomechanism of this process remains unclear. The objective of this study was to investigate the pathomechanism of the ossification process, including the roles of various transcriptional factors in the ossification of human thoracic ligamentum flavum.

Methods: Sections of the thoracic ligamentum flavum were obtained from 31 patients with OLF who underwent posterior thoracic decompression, and from six control patients free of OLF. Cultured ligamentum flavum cells (n = 6, each) were examined with real-time reverse transcription-polymerase chain reaction (RT-PCR) analysis for Sry-type high-mobility group box 9 (Sox9), runt-related transcription factor 2 (Runx2), muscle segment homeobox 2 (Msx2), Osterix, distal-less homeobox 5 (Dlx5), and AP-1. The harvested sections were examined with hematoxylin-eosin, the terminal deoxynucleotidyl transferase-mediated dUTP-biotin nick end-labeling (TUNEL) method, and immunohistochemistry for the transcriptional factors.

Results: Compared with the control, the OLF showed disorganization of the elastic fiber bundles and abundant hypertrophic chondrocytes in the ossification front. TUNEL-positive chondrocytes were found near the ossified plaques. The mRNA expression levels of Sox9, Runx2, Msx2, and AP-1 in cultured cells from the ligamentum flavum of OLF patients were significantly different from those of the control. OLF samples were strongly immunoreactive to Sox9, Runx2, and Msx2 at proliferating chondrocytes in the fibrocartilage area. Hypertrophic chondrocytes were positive for Runx2, Osterix, Dlx5, and AP-1.

Conclusions: The ossification process in OLF seems to involve chondrocyte differentiation under the unique expression of transcriptional factors. Accumulation of hypertrophic chondrocytes was evident around the calcified area at the ossification front, and we suggest that the differentiation of these cells seems to be concerned with the ossification process.

Introduction

Various pathologic conditions are known to result in ossification of the spinal ligament with subsequent neurologic compromise. Ossification of the ligamentum flavum (OLF) is an isolated form of spinal column ossification but also occurs in association with diffuse idiopathic skeletal hyperostosis, ankylosing spondylitis, and metabolic diseases such as Paget disease, hypoparathyroidism, and X-linked hypophosphatemia [1-5]. This clinical entity has been reported almost exclusively in northern East Asian countries, although it has been investigated in other regions, including southern China, India, the Middle East, and Caribbean Islands [6-8]. Although recent advances in radiologic and electrophysiological techniques allow early diagnosis of OLF [9,10], little is known about the spatial progress within the spinal canal, and no standardized treatment is known for OLF.

Several studies have described the possible roles of mechanical, genetic, metabolic, and cell biologic factors in the development and progression of OLF [11-15]. From a histopathologic point of view, enchondral ossification contributes to bone formation in the spinal

* Correspondence: yayama@u-fukui.ac.jp
† Contributed equally
[1]Department of Orthopaedics and Rehabilitation Medicine, Faculty of Medical Sciences, Fukui University, Eiheiji, Fukui 910-1193, Japan
Full list of author information is available at the end of the article

ligaments [16]. The ossification fronts exist between the ossified plaque and the non-ossified fibrous area; they form a multiple-layer structure that includes the fibrocartilage layer, calcification front, calcified-cartilage layer, and ossified region. In our previous studies, we observed disordered orientation of the elastic fibers and expansion of the cartilaginous area in the early stages of ossification in the *twy/twy* mouse, which is known to develop spontaneous spinal ligament ossification [11,17]. In human samples of the ossified spinal ligament, the ossification front includes proliferating small blood vessels and clusters of hypertrophic chondrocytes producing various forms of collagen (such as collagen type II or type X), particularly around the calcification front [18,19]. Thus, we considered that these chondrocytes are involved in the progression of OLF, although these pathologic processes have not yet been elucidated.

The present study is an extension of our previous studies [11,17-19] and was designed to determine the ossification process in human OLF samples. Specifically, we focused on the expression and localization of the transcriptional factors that modulate the properties of fibroblasts-like cells and chondrocytes at the ossification front during the process of ossification.

Materials and methods

Patient population

A total of 31 patients who presented with progressive symptoms and signs of myelopathy and radiologic evidence of OLF (18 men, 13 women; mean age at surgery, 69.0 years; range, 52 to 86 years) underwent posterior decompressive surgery for thoracic OLF between 2001 and 2009. Samples of non-ossified ligamentum flavum obtained from six patients (three men and three women; mean age, 69.8 years; range, 60 to 81 years), who underwent posterior surgery for fracture or disc herniation in the thoracic spine, served as the controls. None of the patients had evidence of congenital bone or joint disorders or musculoligamentous tissue abnormalities. None of the patients was positive for rheumatoid factor, had hyperparathyroidism, or was taking glucocorticoids or bisphosphonate.

Patients had a variable degree of OLF-related spinal-cord impingement posteriorly and posterolaterally (Figure 1a, b). The lesion was categorized as lateral (six cases), extended (seven cases), enlarged (seven cases), fused (six cases), or tuberous (five cases) subtype, based on examination of computed tomography (CT) images taken at the level suspected to be responsible for the myelopathy and the proposed CT classification of thoracic OLF [20,21].

All patients underwent posterior decompressive surgeries: one-level decompression in 19 patients, two-level decompression in 10 patients, and three-level decompression in two patients. A level-specific diagnosis was made based on neurologic signs, CT findings, spinal cord-evoked potentials, and magnetic resonance imaging (MRI: 1.5-Tesla Signa, General Electric, Milwaukee, WI, USA).

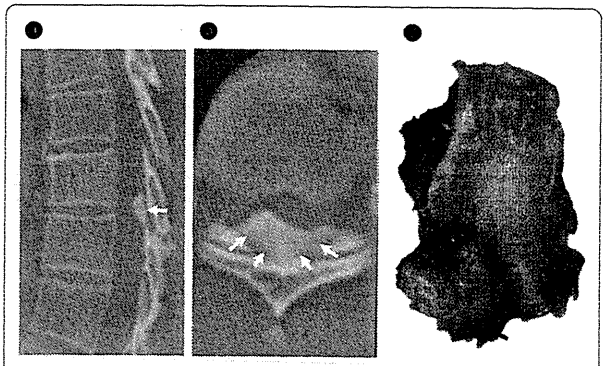

Figure 1 Representative case of tuberous type OLF. Sagittal **(a)** and axial **(b)** CT images obtained in a 72-year-old woman with T11-12 OLF. Note the fusing of the ossified plaque at midline and the progression of this process into the spinal canal. The resected sample **(c)** contains a hard mass from dura mater aspect (arrow, ossification). CT, computed tomography; OLF, ossification of the ligamentum flavum.

The applied surgical technique was described in detail in our previous publication [19]. The OLF sample was obtained through a posterior midline approach followed by exposure of the vertebral laminae and ligamentum flavum. The spinous processes and cortices of the laminae near the OLF lesion were cut or resected, by using either a high-speed surgical drill or a micro-Kerrison rongeur (with a 2-mm blade and 1-mm thickness), under a direct surgical microscope (OPM 16CFC; Carl-Zeiss, Oberkochen, Germany). Because the OLF lesion often extended laterally, just medial to the facet joint, approximately the medial one third of the facet joint at the affected vertebral level(s) was resected, followed by cutting the inner cortex of the far-lateral site of the lamina. The OLF lesion was then isolated and floated like an "island" on the dura mater *vis a tergo*. At that stage, a pair of epidural electrodes (Unique Medical, Tokyo, Japan) was positioned approximately 4 to 6 cm away from the OLF lesion, proximally and distally, for spinal cord monitoring [9]. A pair of fine-tip skin-hooks was then applied to the sides of OLF lesion to lift carefully the ossified plaque dorsally away from the dura mater, before it was finally resected. The dura mater was also sometimes resected even when ossified, but care was taken to preserve the arachnoid membrane.

A written informed consent was obtained from each patient, and the study protocol strictly followed the Human Ethics Review Committee of our University.

Cell culture

Ligament specimens were harvested under aseptic conditions during surgery from six patients (three men and three women; mean age at surgery, 71.0 years; range, 59 to 84 years; four fused type and two tuberous type on CT classification) for cell culture. Samples of non-ossified ligamentum flavum (three men, three women; mean age, 69.8 years; range, 60 to 81 years) were obtained from six patients who underwent thoracic posterior surgeries and served as the control. The tissues surrounding the ligaments were removed carefully under a dissecting microscope, and the ligaments were extirpated carefully from the not-ossified areas to avoid contamination with osteogenic cells. The collected ligaments were minced into approximately 0.5-mm^3 pieces and then plated onto 25-mm^2 culture dishes and maintained in Dulbecco modified Eagle medium supplemented with 10% fetal bovine serum, 100 unit/ml penicillin G sodium, and 100 μg/ml streptomycin sulfate in a humidified atmosphere of 95% air and 5% CO_2 at 37° C. At confluence, the cells were harvested from the dishes with 0.02% ethylenediaminetetraacetic acid (EDTA) and 0.05% trypsin for further passages. The cultured cells were characterized at the third passage. Samples of six control specimens were cultured in a similar fashion.

Real-time reverse transcription-polymerase chain reaction (RT-PCR) analysis

Real-time RT-PCR was used for semiquantitative analysis of the relative mRNA expression levels of transcriptional factors (repeated 3 times for each sample), by using cultured ligamentum flavum cells from six ossified samples and six control non-ossified samples. The cultured cells on each plate were disrupted in a lysis buffer containing β-mercaptoethanol, and the total RNA was purified by using RNAiso Plus (code no. 9108/9109; Takara Biomedicals, Ohtsu, Japan) and treated with DNase I (Takara Biomedicals). Reverse transcription was performed by using 1 μg of total RNA, PrimeScript RT reagent Kit (RR037A; Takara Biomedicals) and a random primer. Real-time RT-PCR was performed on SYBR Premix Ex Taq II (RR081A, Takara Biomedicals) by using 1 μl of the synthesized cDNA and SYBR Green PCR master mix (PE Applied Biosystems, Foster City, CA). The primer sequences used in the present study were Sox9, 5'-ACC AGT ACC CGC ACT TGC AC-3' and 5'-CGC TTC TCG CTC TCG TTC AG-3'; Runx2, 5'-CAC TGG CGC TGC AAC AAG A-3' and 5'-CAT TCC GGA GCT CAG CAG AAT AA-3'; Msx2, 5'-ATG CCA CGC CAG TGG GAT A-3' and 5'-TGC ACG CAG GGT TAG CAG AG-3'; Osterix, 5'-GCC ATT CTG GGC TTG GGT ATC-3' and 5'-GAA GCC GGA GTG CAG GTA TCA-3'; Dlx5, 5'-TAG CTA CGC TAG CTC CTA CCA CCA G-3' and 5'-GGT TTG CCA TTC ACC ATT CTC A-3'; and AP-1, 5'-GGG AAC AGG TGG CAC AGC TTA-3' and 5'-GCA ACT GCT GCG TTA GCA TGA-3'. The target genes were amplified and analyzed in triplicate by using ABI Prism 7000 SDS software. The expression levels of the target genes were estimated relative to that of glyceraldehyde-3-phosphate dehydrogenase (GAPDH).

All data were expressed as mean ± SEM. Differences between groups were examined with the Student *t* test. A *P* value < 5% was considered significant.

Histopathologic processing and immunohistochemical staining

Histopathologic and immunohistochemical examinations were performed as described previously by our group [17-19,22]. The resected OLF plaque together with the surrounding ligament and ligamentous enthesis were bisected midsagittally and then fixed with 10% buffered formaldehyde for 48 hours at 4°C, and further decalcified for 4 to 7 days at 4°C in 0.5 *M* EDTA; and 0.5 *M* Tris-HCl buffer at pH 7.6, and then embedded in paraffin by using standard procedures. Serial 4-μm-thick sagittal sections of the OLF-ligament-enthesis complex were prepared for hematoxylin and eosin (H&E) and elastica van Gieson (EVG) staining.

For immunohistochemical staining, serial 4-μm-thick sections were prepared from the paraffin-embedded specimens, deparaffinized with xylene, and treated with ethanol. After washing with water, the intrinsic peroxidase was blocked with 0.3% H_2O_2-methanol solution at 20°C for 10 minutes and washed with phosphate-buffered saline (PBS; pH 7.4). The sections were irradiated 3 times in a polypropylene side-holder with a cap filled with PBS over a period of 5 minutes, by using a microwave oven (500 W, ER-245; Toshiba, Tokyo). The sections were then reacted with blocking solution (PBS containing carrier protein and 15 mM sodium azide LSAB kit (Lot 00075; Dako, Glostrup, Denmark) at 20°C for 10 minutes. This was followed by reaction with the following primary antibodies at 4°C overnight: rabbit polyclonal anti-Sox9 (DO406; Santa Cruz Biotechnology, Santa Cruz, CA, containing 200 μg IgG in 1 ml PBS with < 0.1% sodium azide and 0.1% gelatin), mouse monoclonal anti-Runx2 (JRH02; R&D Systems, Minneapolis, MN; containing 0.2 μm filtered solution in PBS with 5% trehalose), rabbit polyclonal anti-Msx2 (CO404; Santa Cruz Biotechnology; containing 200 μg IgG in 1 ml PBS with < 0.1% sodium azide and 0.1% gelatin), rabbit polyclonal anti-Osterix (20450; GeneTex, San Antonio, TX; containing 1 mg IgG in 1 ml PBS with 2% sucrose), rabbit polyclonal anti-Dlx5 (1; Proteintech Group, Chicago, IL; liquid solution, PBS with 0.1%

sodium azide and 50% glycerol), and rabbit polyclonal anti-AP-1 (SH0302281; Abgent, San Diego, CA; containing 0.25 mg/ml IgG in 0.4 ml PBS with 0.09% NaN3) antibodies. Sections were further reacted with goat anti-mouse immunoglobulin antibodies and conjugated to peroxidase labeled-dextran polymer (EnVision; peroxidase, mouse, Dako) at 20°C for 45 minutes and then rinsed with PBS at pH 7.4. To visualize the peroxidase color reaction, sections were incubated with DAB-HCl solution (CB090; Dojin Chemicals, Tokyo; 50 mg dissolved in 100 ml of 0.05 *M* TRIS-HCl buffer at pH 7.4) at 20°C for 10 minutes, and then washed in water. Nuclear counterstaining was carried out with hematoxylin.

Terminal deoxynucleotidyl transferase-mediated dUTP-biotin nick-end labeling (TUNEL) staining

Apoptotic cell death was assessed with the TUNEL technique. The specimens were deparaffinized and dehydrated by using standard protocols; the tissue sections (4 μm) were incubated with blocking solution (0.3% H_2O_2 in methanol) for 30 minutes at room temperature. After rinsing with PBS (pH 7.2), the sections were incubated for 15 minutes at 37°C with proteinase K solution (10 μg/ml in 10 mM Tris-HCl buffer, pH 7.4) and rinsed twice with PBS. TUNEL reaction mixture (50 μl enzyme solution (TdT from calf thymus in storage buffer) added to 450 μl labeled solution (nucleotide mixture in reaction buffer) and mixed well to equilibrate components) was prepared immediately before use, placed on slides (50 μl/slide), and incubated for 60 minutes at 37°C. For the negative control, the labeled solution without terminal transferase was placed on slides (50 μl/slide) instead of the TUNEL reaction mixture. These were rinsed 3 times with PBS, added to DAB substrate (10 μl 30% H_2O_2 added to 5 mg/ml DAB in 50 mM Tris-HCl buffer, pH 7.4) and incubated for 10 minutes at room temperature. The slides were rinsed with distilled water and counterstained with methyl green (1%) for 5 minutes. After mounting, the specimens were analyzed under light microscopy.

Transmission electron microscopy

The ligamentum flavum tissue was resected by trimming (1.0 mm^3) and then fixed in 2.5% glutaraldehyde water solution for 2 hours. It was dehydrated with propylene oxide (Nakalai, Kyoto, Japan), and embedded in Epon 812 (Oken, Tokyo). In the final stage, 100-nm-thick ultrathin sections were prepared by using an ultramicrotome (Ultracut N; Reihert, Wien, Austria), and stained with 2% uranyl acetate (50% ethanol solution), and observed under a transmission electron microscope (H-700; Hitachi, Tokyo).

Results

Histopathology, TEM, and TUNEL findings

Macroscopically, the OLF showed round, hard protrusions with a relatively smooth surface at certain regions of the dorsal surface (Figure 1c). The sagittal view showed ossification plaque that extended from the edge of the lower lamina to the upper lamina, without a clear border between the two areas, projecting ventrally into the spinal canal, accompanied by ossification of the dura mater in three (9%) patients.

Microscopically, the control samples contained a thin-layered structure between the fiber and the laminar bone, with uniform arrangement of the fibers (Figure 2a). In OLF samples, the ossification fronts included the fibrocartilage layer, calcification front, and the calcified cartilage layer, where significant irregularities and several disruptions were prominent attributes (Figure 2b). This irregularity extended not only along the longitudinal direction of the fibers but also in other directions. In addition, a significant number of chondrocytes were present around the calcification front. Around the ossification front, osteoblasts were found, just near the ossified layer, and a gathering of infiltrative small blood vessels with mesenchymal cells (Figure 2c, d). Although elastic fibers had a regular arrangement in control samples, they showed irregular arrangement, abnormally small diameter of fragmented elastic fibers, and abundant thick bundles of collagen fibers in OLF samples (Figure 2e, f). These histopathologic findings were observed to a greater or lesser degree in all patients, being more severe in larger ossified plaques (especially in the enlarged, fused, and tuberous subtypes).

Under TEM examination, OLF samples showed the disappearance of the elastic fiber structures as well as an increase in fibrotic tissue, compared with the controls (Figure 3a, b). Matrix vesicles containing electron-dense material were also seen near the chondrocytes (Figure 3c). TUNEL-positive chondrocytes with pigmented and condensed nuclei were found around the ossification plaque, representing apoptotic cells (Figure 3d, e). In particular, TUNEL-positive chondrocytes were mostly seen in the areas close to the calcification front, especially in large ossified plaques, such as the fused and tuberous types.

Cultured cells and real-time RT-PCR analysis

A portion of the cells from the OLF samples showed spindle-shaped morphology, being arranged in several layers. In the control samples, cultured cells also showed spindle-like morphology (Figure 4a, b).

Figure 4c shows the relative mRNA expression levels of six transcriptional factors in cultured ligamentum flavum cells by using real-time RT-PCR analysis. The

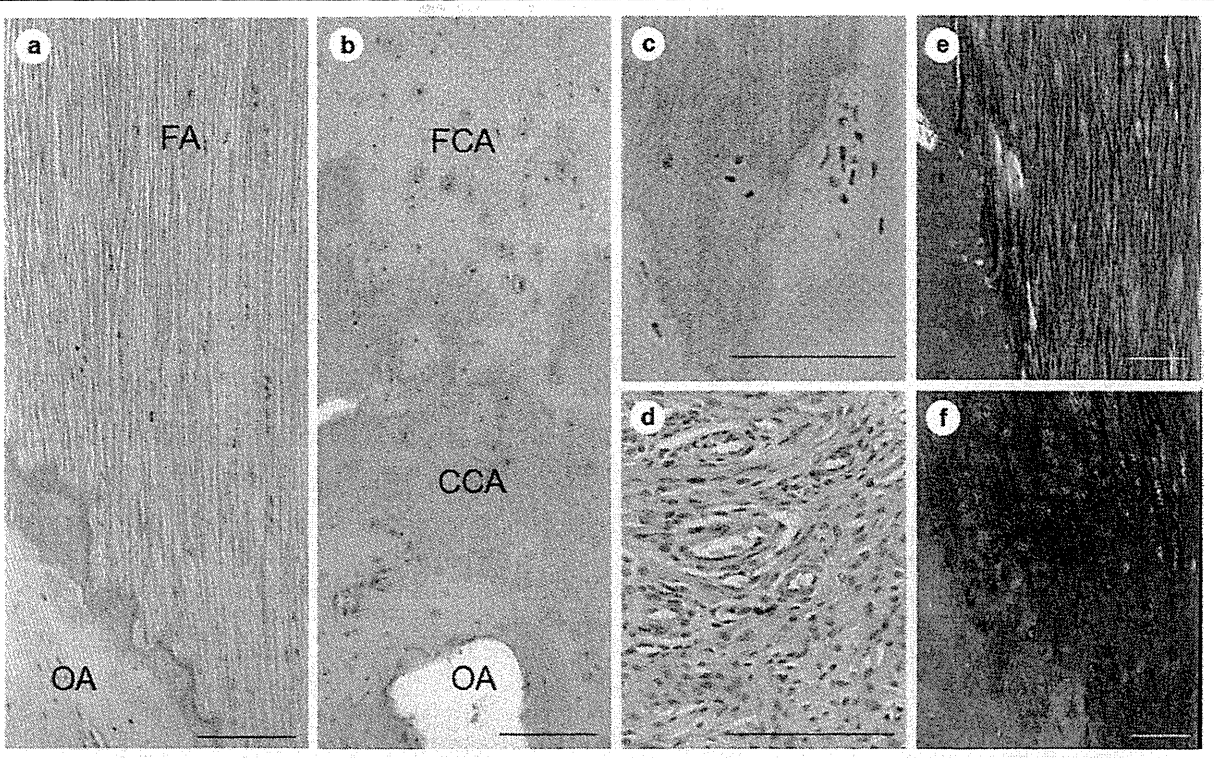

Figure 2 Histologic examination of the ossification front. Section of the control ligamentum flavum **(a)** showing a thin ossification front and regular arrangement of fiber bundles. In OLF samples (representative case of fused type), note the expanding ossification front, gathering many chondrocytes, and featuring an irregular of calcification front **(b)**. In addition to the ossification front, note the presence of osteoblasts as well as small blood cells with mesenchymal cells **(c, d)**. In the EVG image, elastic fibers exhibit a regular arrangement **(e)**, whereas the OLF samples contained irregular, fragmented fibers or no elastic fibers **(f)**. **(a-d)** H&E; **(e, f)** EVG staining. CCA, calcified cartilage area; EVG, Elastica van Gieson; FA, fiber area; FCA, fibrocartilage area; OA, ossified area; OLF, ossification of the ligamentum flavum. Scale bar = 100 μm.

mRNA expression levels (relative to the control sample) in the OLF sample were 2.7 ± 0.05 for Sox9, 1.7 ± 0.1 for Runx2, 2.2 ± 0.2 for Msx2, 1.2 ± 0.9 for Osterix, 1.0 ± 0.9 for Dlx5, and 1.9 ± 0.2 for AP-1. The relative mRNA expression levels of Sox9, Runx2, Msx2, and AP-1 in OLF samples were significantly higher than those in the control group ($P < 0.05$, each). However, the mRNA expression levels of Osterix and Dlx5 were not significantly different from the control.

Immunohistochemical findings

In 23 of 31 OLF patients, the chondrocytes present in the ossification front were immunopositive for Sox9; the immunoreactivity was strictly limited to proliferating chondrocytes in the fibrocartilage area, whereas the hypertrophic chondrocytes close to the calcification front were negative for Sox9 (Figure 5a). Conversely, Sox9 expression was significant in mesenchymal cells present around the ossification front, where the ligamentous matrix showed degenerative changes in these patients. Runx2 expression was evident in 20 of 31 cases and localized in proliferating chondrocytes and hypertrophic chondrocytes (Figure 5b). Immunopositivity for Msx2 was noted in 24 of 31 cases and localized in proliferating chondrocytes, and in particular, the mesenchymal cells near the ossification front were strongly positive for Msx2 (Figure 5c). Positive immunostaining for Osterix was noted in 16 of 31 cases and localized in chondrocytes present in the calcified cartilage layer and fibrocartilage layer. Furthermore, numerous Osterix-positive hypertrophic chondrocytes were seen around the calcification front (Figure 6a). Immunostaining for Dlx5 was significant in 12 of 31 cases, and that for AP-1 was in 14 of 31 cases in hypertrophic chondrocytes in the calcified cartilage area (Figure 6b, c). The immunohistochemical expression of these factors is summarized in Additional files 1 and 2.

Discussion

Ligamentum flavum is a longitudinally arranged two-layered structure lining the posterior aspect of the spinal canal and functionally allows flexibility and stabilization of the spine [23]. The normal ligament is highly elastic, based on the large proportion of elastic fibers,